P • A • R • T • 2

SOIL MECHANICS AND FOUNDATION DESIGN PARAMETERS

SECTION 2A
SOIL MECHANICS

RICHARD W. STEPHENSON

2A.1 INTRODUCTION

Rock consists of an aggregate of natural minerals joined by strong and permanent cohesive bonds. *Rock mechanics* is the engineering study of rock.

Soil is defined as natural materials consisting of individual mineral grains not joined by strong and permanent cohesive forces. Natural soils are products of the weathering of rock. *Soil mechanics* is the study of the engineering properties of soil.

2A.2 PHYSICAL CONDITION

2A.2.1 Introduction

A natural soil consists of three separate components: solids, liquids, and gases. The solids are normally natural mineral grains, although they can be human-made materials such as furnace slag or

mine tailings. The liquid is usually water, and the gas is usually air. The relative amounts of each of the components in a particular soil may be expressed as a series of ratios. These ratios may be based on relative masses or weights, relative volumes, or relative mass or weight densities. These weight–volume ratios are fundamental to soil mechanics and geotechnical engineering.

2A.2.2 Two-Phase Soil (Dry or Saturated)

If a soil consists of only solids (mineral particles) and voids (either gas- or liquid-filled), then it is a two-phase soil system. Although the void spaces are interspersed throughout the mineral particles, a unit volume of the soil may be viewed as in Fig. 2A.1. Using this figure, some terms can be defined. The unit weight of soil solids (γ_s) is

$$\gamma_s = \frac{W_s}{V_s} \tag{2A.1}$$

where W_s = weight of solid phase
V_s = volume of solid phase

The unit weight of the total soil system (γ_t) is

$$\gamma_t = \frac{W_t}{V_t} \tag{2A.2}$$

where W_t = total weight
V_t = total volume

If the voids are filled with gas (air), then

$$W_v = 0$$
$$\gamma_t = \gamma_{\text{dry}} = \frac{W_s}{V_t} \tag{2A.3}$$

where γ_{dry} = dry unit weight

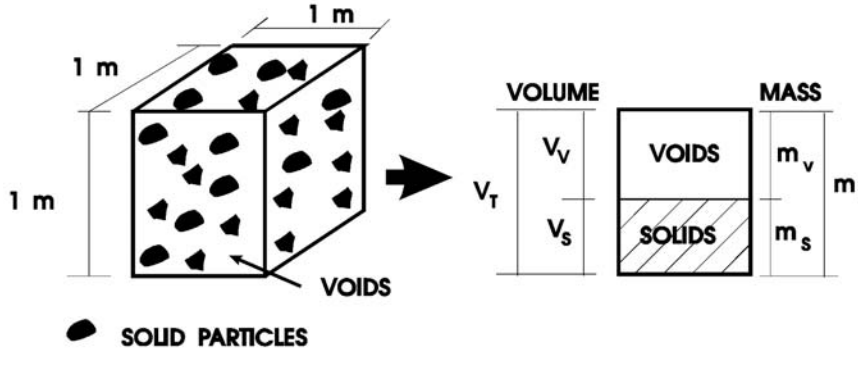

FIGURE 2A.1 Two-Phase representation of soil.

If the voids are filled with liquid (water)

$$W_v = W_w$$
$$\gamma_t = \gamma_{sat} = \frac{W_s + W_w}{V_t} \tag{2A.4}$$

where γ_{sat} = saturated unit weight
W_w = weight of water
The buoyant unit weight is defined as:

$$\gamma' = \gamma_{sat} - \gamma_0 \tag{2A.5}$$

where γ_0 = unit weight of water
= 62.4 pcf = 9.807 kN/m^3
The voids ratio (e) is

$$e = \frac{V_v}{V_s} \tag{2A.6}$$

where V_v = volume of voids
Porosity (n%)is defined as

$$n\,(\%) = \frac{V_v}{V_T} \times 100 \tag{2A.7}$$

Water content (w%) is

$$w\,(\%) = \frac{m_w}{m_s} \tag{2A.8}$$

Specific gravity of soil solids (G_s):

$$G_s = \frac{\gamma_s}{\gamma_0} \tag{2A.9}$$

2A.2.3 Three-Phase Soil

Soils are not always either dry or saturated. Often, the voids are partly filled with water. The soil block then consists of a three-phase system, as shown in Fig. 2A.2. Using Fig. 2A.2, some weight-volume relationships can be defined. Moist unit weight is

$$\gamma_{moist} = \frac{W_t}{V_T} \tag{2A.10}$$

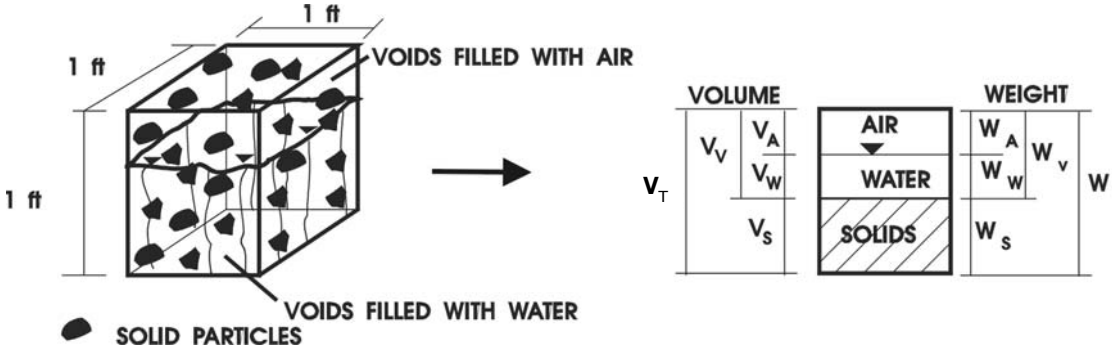

FIGURE 2A.2 Three-phase soil system.

Water content (w%) is

$$w\,(\%) = \frac{W_w}{W_s} \tag{2A.11}$$

Degree of saturation is

$$S_r = \frac{V_w}{V_V} \times 100 \tag{2A.12}$$

2A.3 SOIL IDENTIFICATION AND CLASSIFICATION

2A.3.1 Introduction

Soil is identified and classified using several systems. These systems include (a) the method by which the solid particles are formed; (b) the size of the individual particles; and (c) the engineering properties of the soil.

2A.3.1.1 Soil Formation

Soil can be classified based on the origin of their constituents. The major origins or soil are rock weathering and organic decomposition.

Rock Weathering. Rock weathering can be either mechanical or chemical. Either will result in a large rock mass being broken into smaller particles.

Mechanical weathering. Mechanical weathering can be caused by exfoliation of large rock masses, differential thermal expansion and contraction of minerals within a rock mass, or the freezing and subsequent thawing of water in minute fissures in the rock mass. In addition, mechanical weathering can be caused by the impact by running water on a rock mass, scouring of a rock mass by glacial movement, or breakdown of the rock mass by the impact of wind-blown particles. Rocks are also weathered by the expansion of the roots of vegetation growing in the minute cracks and fissures in the rock.

Chemical Weathering. Chemical weathering occurs when hard rock minerals are transformed into soft, easily erodible matter. The primary chemical processes that weather hard rock minerals include oxidation, carbonation, hydration, and leaching. When a rock containing iron comes into con-

tact with moist air, $2Fe_2O_3 \cdot H_2O$ ("rust") is formed. This rust is very soft and easily eroded from the rock mass.

When water is added to CO_2 in the atmosphere, a weak carbonic acid is formed. This acid decomposes minerals containing iron, calcium, magnesium, sodium, or phosphates.

Hydration. Hydration is the taking up of water, which is then bound chemically to form new minerals. Not only does hydration alter the mineral, often to a softer state, but it also causes a volume increase that in turn increases the decomposition of the rock mass.

When water comes into contact with salt, gypsum, feldspars, or limestone, the minerals will dissolve. The dissolved minerals are then transported and redeposited elsewhere. This is called *leaching*.

Organic Decomposition. Because organic soils are so unique and difficult to deal with, only a relatively small fraction of the soil solids needs to be organic for the organic constituent to control its engineering behavior.

Peat. Peat is formed by the growth and subsequent decay of plants. These soils tend to be fibrous, black in color, and smell like rotten eggs.

Coral. Coral is the accumulation of fragments of inorganic skeletons or shells of organisms. These soils are easily identified visually.

2A.3.1.2 Mineralogy

A mineral is an inorganic compound found in nature. For engineering purposes, the minerals are separated into rock and soil minerals.

Quartz. Quartz is the principal mineral in granite, sands, and rock flour. The mineral is colorless, transparent, and quite hard. Quartz is very resistant to chemical weathering. Quartz has a specific gravity of 2.66.

Feldspar (Silicates of Aluminum). Feldspars are important because these minerals chemically weather into clay minerals. Their specific gravities are about 2.7.

Micas. Micas are the primary mineral in granites and gneiss. Mica can be split into thin, elastic sheets. It is colorless and transparent and has a specific gravity of 2.8.

Carbonates. Carbonates are derived from the chemical weathering of calcium-bearing feldspars and other calcium-bearing rocks and have been reformed into new rock masses. Principal carbonates include calcite, dolomite, and the various limestones. The carbonates and quite soft and white to colorless and are highly susceptible to chemical weathering. Their specific gravities vary from 2.7 to 2.8.

Principal Clay Minerals. The principal clay minerals are listed below.

Kaolinite. Kaolinite is derived from the chemical weathering of feldspars and other aluminum-bearing rocks. Its primary structure consists of a single sheet of gibbsite bound to a sheet of silicon (Fig. 2A.3). Successive two-layer sheets are bound together by weaker hydrogen bonds. These hydrogen bonds can be relatively easily broken, yielding a basic two-layer sheet structure.

Illite. Illite takes the structure of kaolinite a further step. The hydroxyls of the octahedral layer are stripped of their hydrogen ions on both sides, and the oxygen ion is the tip of a tetrahedral layer on both sides of the octahedral layer. The octahedral layer is electrically neutral. However, the tetrahedra are not neutral. Approximately one tetrahedron in seven contains an aluminum (+3) in place of the usual silicon (+4) because of isomorphous substitution. This results in an overall charge deficiency in each of the tetrahedral layers. This charge deficiency draws potassium ions (+1) into the structure in that octagonal void that exists, as discussed previously. Thus, a potassium ion fits into this void and the void of the next sheet of illite. It is drawn by the negative charge of the tetrahedral layer and thereby holds the sheets together. This bond is obviously not as strong as the hydrogen bond of kaolinite, but it is not weak either.

Montmorillonite (Smectite). The make-up of montmorillonite is very similar to that of illite. Montmorillonite is a three-layer mineral, except the tetrahedral layer is relatively neutral with almost no substitution of aluminum for silicon. The octahedral layer has charge deficiencies with alu-

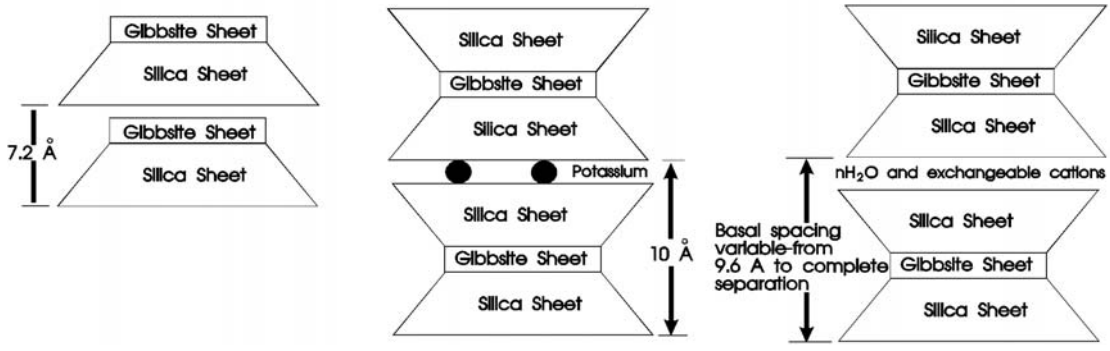

FIGURE 2A.3 Structure of principal clay minerals: (a) kaolinite, (b) illite, (c) montmorillonite.

minum in the vacated positions. Since the seat of the charge deficiency is in the center of the sheet, there is a weaker attraction by the negative charge to outside positive charges. Instead of strongly attracting potassium, hydrated ions, such as sodium, are weakly attracted. The sodium ions are weakly attracted to the potassium ions and to the negative faces of the sheets of montmorillonite because of its dipole nature. Thus montmorillonite surrounds its sheets with oriented water and hydrated cations. Soils with montmorillonite are known for their propensity to swell in the presence of water.

2A.3.1.3 Grain (Particle) Size Classification

One method of classifying soils is by the size of the individual particles. The size and distribution of soil particles are determined by performing a grain size analysis.

Coarse-Grained Soils. Coarse-grained soils behave in nature as individual particles. They are subdivided into gravel and sand. *Gravel soils* have a particle sizes coarser (larger) than about the #4 or the #10 mesh sieve opening, depending upon which particular classification system is used. *Sands* have particle sizes finer than gravel (#4 or #10 mesh) and coarser than the #200 mesh sieve. Coarse sand particles pass the #4 sieve and are retained on the #10 mesh sieve. Medium sand has a particle size that is smaller than the #10 and larger than the #40 mesh. Fine sand has particles in the #40 to the #200 mesh size.

Fine-Grained Soils. Fine-grained soils largely behave as a mass and not as individual particles. Their particle sizes can be divided, however, into silt and clay. *Silt* particles are smaller than the #200 mesh (0.0074 mm) but larger than 2 μm. Silts are derived by the mechanical weathering of rock. *Clay* particles are smaller than 2 μm. They are developed by the chemical weathering of rock minerals.

2A.3.1.4 Grain (Particle) Size Distribution

The particle size distribution analysis of a soil involves determining the relative amounts of particles within given size ranges in a soil mass. Different test methods are used for coarse-grained soils and fine-grained soils.

The particle size distribution of a coarse-grained soil is determined by a sieve analysis (ASTM D-422). The test uses a set of calibrated sieves, stacked in descending opening size, through which the soil is passed. The largest screen opening is several inches and the smallest size commonly used is #200 mesh (0.074 mm). Intermediate size screens are used to separate various sizes of particles down to #200 mesh. Larger particles are retained on the upper sieves, whereas the smaller particles pass through onto the lower sieves. The grain size distribution of coarse-grained soils influences their density, permeability, shear strength, and compressibility.

The grain size distribution of fine-grained soil is determined by sedimentation. The method is based on Stoke's Law:

$$D = \sqrt{\frac{18\eta v}{\gamma_s - \gamma_f}} \tag{2A.13}$$

where: D = diameter of sphere
η = viscosity
v = velocity of fall of sphere
γ_s = unit weight of sphere
γ_f = unit weight of fluid

A sample of the soils is mixed into a suspension in water and the suspension placed in a sedimentation cylinder. Using Stoke's Law, it is possible to calculate the time t for particles of diameter D to settle a specified depth in the suspension. A hydrometer is used to measure the specific gravity of the suspension. Details of the test are given in ASTM D 422.

Although the grain size distribution of fine-grained soils is often performed, their properties are more affected by structure, shape, and geologic origin than particle size distribution.

The distribution of particle sizes in a soil is represented by a *grain size distribution curve*. This curve is a semilogarithmic plot with the ordinates being the percentage by weight of particles smaller than the size given by the abscissa (Fig. 2A.4). The flatter the distribution curve, the larger the range of particle sizes in the soil. The steeper the distribution curve, the smaller the size range. A soil that has a relatively even distribution of particle sizes is called a *well-graded soil*. A soil that consists primarily of particles of one size is called *uniform*. Descriptive coefficients are used to quantify various characteristics of the grain size distribution curve.

The particle size corresponding to any specified value on the ordinate (percent smaller) curve can be read on the size distribution curve For example, the diameter of particle that corresponds to

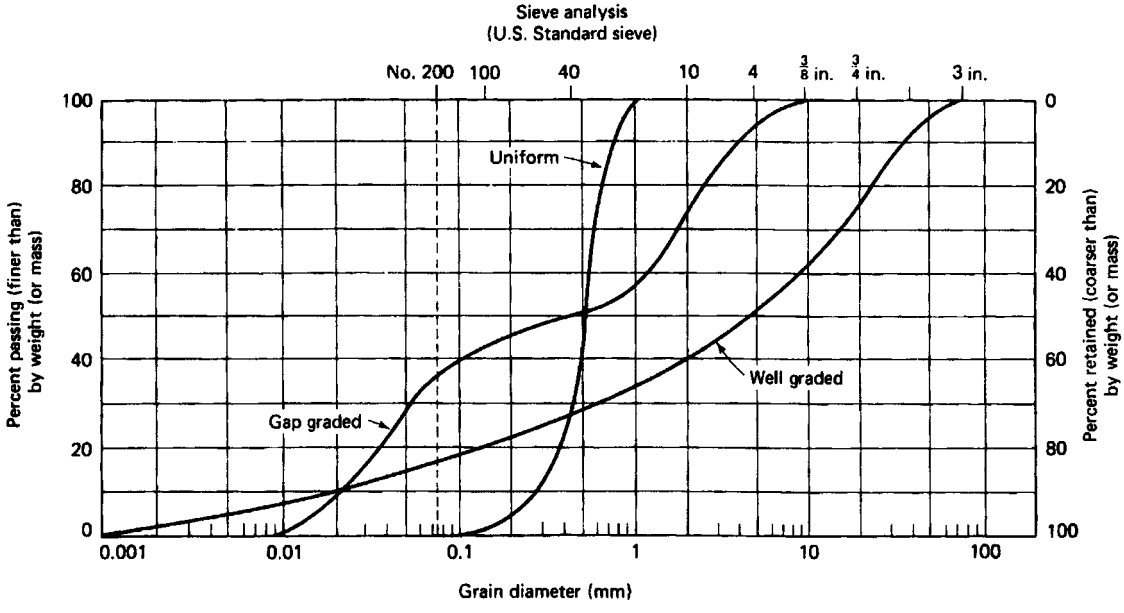

FIGURE 2A.4 Typical grain size distribution curves.

the 50% smaller ordinate is the D_{50} size. Similarly, the D_{10} size is the diameter of grains that only 10% of the soil is finer than. The D_{10} is known as the effective diameter of the soil.

The uniformity coefficient is defined as:

$$C_u = \frac{D_{60}}{D_{10}} \tag{2A.14}$$

and is a measure of the general slope of the grain size distribution curve. A C_u near unity indicates a one-size (uniform) soil. On the other hand, a $C_u = 6$ indicates a well-graded soil.

The coefficient of curvature (C_z) indicates the constancy of the slope of the grain size distribution curve.

$$C_z = \frac{D_{10}^2}{D_{60} \times D_{10}} \tag{2A.15}$$

A C_z of between 1 and 3 indicates a well-graded soil. C_z values outside these limits indicate either uniform or gap-graded soils.

2A.3.1.5 Grain Shape

Coarse-Grained Soils. The shape of individual coarse-grained soil particles (larger than the #200 mesh) can be classified as being bulky, platey, or needle-like in shape. *Bulky-grained* particles are roughly equidimensional, i.e., the length ≈ width ≈ height. This is true of most gravels, sands, and silts. Bulky-grained soils are strong and relatively incompressible. Sands that are derived from mica have shapes that are *plate shaped*, i.e. length ≈ width ≫ thickness. Platey particles are more elastic and prone to breakage than are bulky-grained particles. Some coral and some clays have particle shapes that are *needle shaped*. These particles are resilient under low static loads but tend to break under higher loads.

Particle Angularity. Under load, angular corners crush and break but resist displacement. Smoother particles are less resistant to displacement but are less likely to crush. Particles are classified as angular, subangular, subrounded, rounded, or well rounded.

Fine-Grained Soils. Silts are products of the mechanical weathering of rock, and therefore their shape is primarily bulky. Because the clay minerals are crystalline with an orderly, sheet-like molecular arrangement, the clay particles break down into very small (<2μm) sheets where the length ≈ width ≫ thickness.

2A.3.1.6 Soil Plasticity

Soil plasticity is defined as the ability to undergo deformation without rupture. Plasticity of a soil is caused by presence of plate-shaped clay particles in the soil. The negative charges on the surfaces of the clay platelets attract and bind polar water molecules to their surfaces. The negative end of the water dipole similarly attracts other water molecules. This phenomenon continues with the attractive forces decreasing at larger distances from the clay surface. This layer of tightly bound water around the clay particle is known as absorbed water. The absorbed water thickness will vary depending upon the strength of the surface charge as well as the presence of cations in the water phase (Fig. 2A.5).

Atterberg Limits. The clay particles are held together by a number of different forces including electrical attraction, hydrogen bonding, cation sharing, and Van Der Wall's forces. When the particles are relatively far apart, there is relatively little particle-to-particle attraction. Therefore, it is relatively easy for particles to slip past each other. However, as the particle spacing reduces due to an applied force or the removal of water, the interparticle attraction will increase and the slip potential between the particles will reduce.

As a clay slurry is reduced in volume by desiccation, it passes from a liquid phase through a vis-

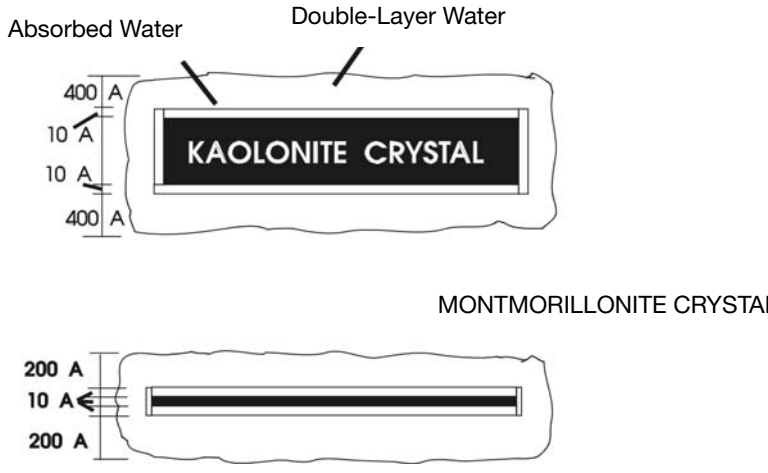

FIGURE 2A.5 Clay particle.

cous fluid stage, through a plastic stage, and finally to a solid state as the particle-to-particle attraction forces increase and the slip potential decreases. Atterberg[1] divided these ranges arbitrarily into five ranges as defined by the water content of the slurry. Two important ranges for engineering work are defined by three limits listed below.

Liquid Limit. The liquid limit (LL) is defined as the lower limit of viscous flow. Casagrande[2] defined the LL as the water content at which a 2 mm wide trapezoidal groove cut in moist soil held in a special cup would close 0.5 inch along the bottom after 25 taps on a hard rubber plate (ASTM D-4318).

Plastic Limit. The plastic limit (PL) is defined as the lower limit of the plastic range, and is the water content at which a sample of soil begins to crumble when rolled into a thread ⅛ inch in diameter (ASTM D-4318).

Shrinkage Limit. The shrinkage limit is the lower limit of volume change upon drying, and is defined as the water content at which the soil is at a minimum volume as it dries out from saturation (ASTM D-4943).

Index properties are used to provide relative measures of the plasticity of a soil. The *plasticity index* (PI) is defined as

$$\text{PI} = \text{LL} - \text{PL} \tag{2A.16}$$

The *liquidity index* is defined as:

$$I_L = \frac{w_n - PL}{PI} \tag{2A.17}$$

The *activity number* (A) is applied to plastic soils in reference to their propensity for undergoing volume change in the presence of varying moisture conditions:

$$A = \frac{PI}{\%\ < 0.002\ \text{mm}} \tag{2A.18}$$

TABLE 2A.1 Typical Values of Activity

Mineral	Activity
Kaolinite	0.2–0.4
Illite	0.5–0.9
Calcium montmorillonite	1.0–2.0
Sodium montmorillonite	4 or more

Uses of the Atterberg Limits. In general, the index properties are indicative of remolded soil properties. The liquid limit indicates compressibility, geologic history of the deposit, and the undrained shear strength, among other things.

Clay mineralogy. Since the clay content (fraction smaller than 0.002 mm) governs the Atterberg limits of a soil, the Atterberg limits are thus an indicator of the type of clay mineral. The activity (A) number is used to estimate the type of clay mineral in a soil (Table 2A-1).

Volume change potential. The propensity for a clay soil to undergo expansion or shrinkage with increases or decreases in moisture content can be estimated using the Atterberg limits (Table 2A.2). As the plasticity index increases and the shrinkage limit decreases, volume change potential increases (Table 2A.3).

Compressibility. Skempton[3] developed a statistical relationship between the liquid limit and the compression index for remolded soils:

$$C_c = 0.007(LL - 10) \tag{2A.19}$$

Research at Cornell[4] has justified the Terzaghi expression for undisturbed, normally consolidated soils:

$$C_c = 0.007(LL - 10) \tag{2A.20}$$

These expressions apply only to normally consolidated soils and are valid to about ±30%.

Geologic History. A plot of liquidity index versus depth will tend to smooth out depositional differences between soils. Deposits with a common depositional history show a smooth curve. A normally consolidated deposit will show a continuous decrease in liquidity index with depth.[5] A plot of liquidity index versus vertical effective consolidation pressure provides a means of estimating whether or not the soil has been overconsolidated.

Undrained Shear Strength. For normally consolidated soils, the curve of water content versus logarithm of effective vertical consolidation pressure, $\bar{p}$, and water content versus logarithm of undrained shear strength, s_u, are parallel. Thus, for a normally consolidated soil, the ratio of $s_u/\bar{p}$ is a constant. Skempton developed a statistical relationship between plasticity index and $s_u/\bar{p}$:

$$\frac{s_u}{\bar{p}} = 0.11 + 0.0037PI \tag{2A.21}$$

TABLE 2A.2 Swell Potential

LL	Swell Potential
0–30	Slight to low
31–50	Moderate to intermediate
>50	High

TABLE 2A.3 Estimation of volume change potential from Atterberg Limits

Plasticity index	Shrinkage limit	Probable expansion, % total volume change dry to saturated	Degree of expansion
>35	<11	>30	Very high
25–41	7–12	20–30	High
15–28	10–16	10–20	Medium
<18	>15	<10	Low

This expression is valid for normally consolidated soils tested in situ by vane shear and for soils tested in unconfined compression.

2A.3.1.7 Soil Aggregate Properties

Primary Structure. Soil structure is the arrangement of individual soil grains in relation to each other. Terzaghi classified soils into three broad classes: cohesionless, cohesive, and composite soils.

Cohesionless soils. Cohesionless soils consist of particles of gravel, sand, or silt, depending upon the size of their individual particles. The structure of these soils can take two forms: single-grained or honeycombed.

Single-grained. Gravel, sand, or silt particles greater than about 0.02 mm settle out of suspension in water as individual grains independent of other grains. Their weight causes the grains to settle and roll to equilibrium positions practically independent of other forces. The particles may come to equilibrium in a loose condition, a dense condition, or anywhere in between (Figure 2A.6). Relative density is used to measure the compactness of a single-grained soil.

$$D_r = \frac{e_{\max} - e}{e_{\max} - e_{\min}} \times 100 \tag{2A.22}$$

A soil that is in its most dense condition will have a relative density of 100%. Vibration can cause rapid reduction of the volume of a loose single-grained soil structure.

Honeycombed. When silt grains with diameters between 0.0002 and 0.02 mm settle out of suspension, molecular forces at the contact areas between particles may be large enough compared to

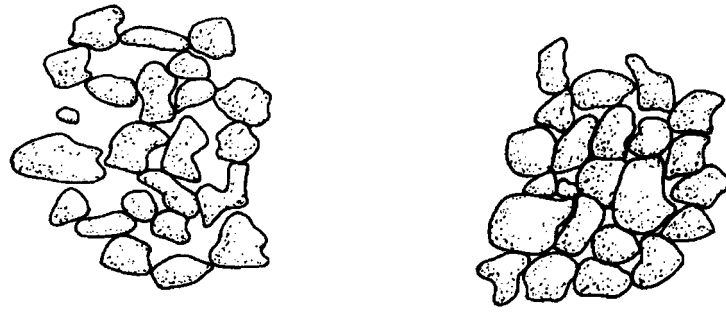

FIGURE 2A.6 Typical single-grained soil structure.

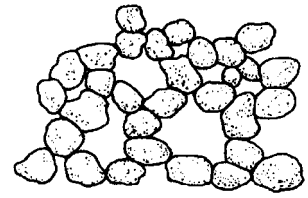

FIGURE 2A.7 Honeycombed structure.

the submerged unit weight of the grains to prevent the grains from rolling down immediately to positions of equilibrium among other grains already deposited. Electrostatic and other forces can cause miniature arches to form, bridging over large void spaces (Figure 2A.7). Because the particles themselves are strong, these honeycombs are capable of carrying relatively large static loads without excessive volume change. However, if the load increases beyond the soil's critical value, large and rapid volume decrease will occur.

Cohesive Soils. Cohesive soils are fine-grained soils whose particles form either a flocculated or dispersed structure.

Particles smaller than 0.0002 mm will not settle out of solution individually due to the Brownian motion. However, because of the electrical charges that exist on the surfaces and edges of clay particles, the negatively charged surfaces are attracted to the positively charged edges and relatively large edge-to-face aggregates or flocs are formed. These flocs grow to masses great enough to settle out of suspension and form *flocculated soils* (Figure 2A.8(a)).

If a flocculated soil is remolded, then the edge-to-face structure collapses and the particles slip into nearly parallel positions. In this configuration, there is very little particle-to-particle contact. This structure is called an *oriented or dispersed structure* (Figure 2A-8(b)).

Composites. In natural clays that contain a significant proportion of larger particles, the structural arrangement of the particles can be highly complex. Single grains of silt and/or sand can be interspersed within a clay platelet matrix.

Consistency and sensitivity of clays. Consistency is a measure of the degree with which a clay soil will resist deformation when loaded. Consistency of clay is measured by the unconfined compression test, which will be described later. Table 2A.4 is often used to describe the consistency of clay.

Sensitivity describes the loss of strength of a soil upon remolding. Numerically, it is defined as the unconfined compressive strength of the undisturbed soil (q_u) divided by the unconfined compressive strength of the same soil remolded at an identical water content (q_r). Table 2A.5 classifies soils according to their sensitivity.

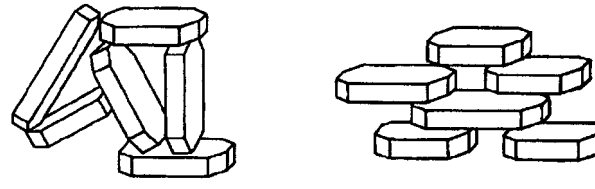

FIGURE 2A.8 Soils that are (a) flocculate; (b) dispersed.

TABLE 2A.4 Consistency of Clay Soils

Consistency	Unconfined compressive strength (tsf)
Very soft	<1/4
Soft	1/4 to 1/2
Medium	1/2 to 1
Stiff	1 to 2
Very stiff	2 to 4
Hard	>4

2A.3.2 Soil Classification

Soil classification is the placing of a soil into a group of soils, all of which exhibit similar characteristics.

2A.3.2.1 Classification According to Origin of Natural Deposits

All soils are either residual or transported.

Residual Soils. Residual soils are formed when rock weathers faster than erosion can carry the soil particles away. In these soils, all soluble materials have been leached out. The chemical disintegration becomes less active with depth, and the alteration becomes less and less with depth until the parent rock is reached. These soils tend to be highly mixed-grained, with gravel or cobble-sized remnants of chemically resistant rock intermixed with clay particles. The particles tend to be very angular.

Transported Soils. Transported soils consist of soil particles that have been moved from their original location by various agents and redeposited. The types of deposits are classified according to their erosion and transportation methods.

Aeolian deposits are wind-transported and deposited. Aeolian deposits are characterized by their high degree of sorting (all-one-size particles) and the uniformity of the deposits. Principal aeolian soils include sand dunes and loess (wind-deposited silt).

Gravitational deposits are soil deposits that have collected at the base of mountains. Chief among the gravitational deposits is talus, which is the accumulation of rock and soil that builds up at the base of cliffs.

2A.3.2.2 Engineering Soil Classification

AASHTO Soil Classification. The American Association of State Highway and Transportation Officials (AASHTO) soil classification identifies kinds of soil in terms of their suitability to serve as a highway base course. This system classifies soils into one of eight groups: A-1 through A-8 (Table 2A-6). A-1 soils consist of well-graded gravels and sands and are the best soils for high-

TABLE 2A.5 Sensitivity of Clay Soils

Sensitivity	q_u/q_r
Insensitive	<1.0
Low	1.0 to 2.0
Medium	2.0 to 4.0
Sensitive	4.0 to 8.0
Extra	8.0 to 10.0
Quick	>10.0

way subgrades. Organic soils that are highly unsuitable for use as a subgrade are classified as A-8. Some groupings are further subdivided. The classifications are based on the soil's grain size distribution and plasticity of the fraction passing the #40 sieve.

The Unified Soil Classification System. This is based on the work of Casagrande.[6] This system classifies soils into three major groups based on their predominant particle size and plasticity. Soils are coarse-grained (sand or gravel) if 50% or more of the soil particles by weight are

TABLE 2A.6 AASHTO soil classification system

TABLE 1 Classification of Soils and Soil-Aggregate Mixtures

General Classification	Granular Materials (35% or less passing No. 200)			Silt-Clay Materials (More than 35% passing No. 200)			
Group Classification	A-1	A-3[A]	A-2	A-4	A-5	A-6	A-7
Sieve analysis, % passing:							
No. 10 (2.00 mm)	...	...	...	...	...	...	...
No. 40 (425 μm)	50 max	51 mm	...	...	...	...	...
No. 200 (75 μm)	25 max	10 max	35 max	36 mm	36 mm	36 mm	36 mm
Characteristics of fraction passing No. 40 (425 μm):							
Liquid limit	...	...	[B]	40 max	41 mm	40 max	41 mm
Plasticity index	6 max	N.P.	[B]	10 max	10 max	11 mm	11 mm
General rating as subgrade	Excellent to Good			Fair to Poor			

[A]The piecing of A-3 before A-2 is necessary in the "left to right elimination process" and does not indicate superiority of A-3 over A-2.

[B]See Table 2A.6B for values.

Reprinted with pennission of American Association of State Highway and Transportation Officials.

TABLE 2 Classification of Soils and Soil-Aggregate Mixtures

General Classification	Granular Materials (35% or less passing No. 200)							Silt-Clay Materials (More than 35% passing No. 200)			
	A-1		A-3	A-3				A-4	A-5	A-6	A-7
Group Classification	A-1-a	A-l-b		A-2-4	A-2-5	A-2-6	A-2-7				A-7-5 A-7-6
Sieve analysis, % passing:											
No. 10 (2.00 mm)	50 max	...	...	...	...	...	...	...	...	...	...
No. 40 (425 μm)	30 max	50 max	51 mm	...	...	...	...	...	...	...	...
No. 200 (75 μm)	15 max	25 max	10 max	35 max	35 max	35 max	35 max	36 mm	36 mm	36 mm	36 mm
Characteristics of fraction passing No. 40 (425 μm):											
Liquid limit	...	...	40 max	41 mm	40 max	41 mm	40 max	41 mm	40 max	41 mm	
Plasticity index	6 max		N.P.	10 max	10 max	11 mm	11 mm	10 max	10 max	11 mm	11 min[A]
Usual types of significant constituent materials	Stone Fragments, Gravel and Sand		Fine Sand	Silty or Clayey Gravel and Sand				Silty Soils		Clayey Soils	
General rating as subgrade	Excellent to Good							Fair to Poor			

[A]Plasticity index of A-7-5 subgroup is equal to or less than *LL* minus 30. Plasticity index of A-7-6 subgroup is greater than *LL* minus 30 (see Fig. 1).

Reprinted with permission of American Association of State Highway and Transportation Officials.

larger than the #200 mesh sieve. Soil are fine-grained (silt or clay) if 50% or more of the soil particles by weight are smaller than the #200 mesh sieve. If the soil contains organic matter, the soil is designated either organic or peat, no matter what the size of the mineral grains. Each class of soil is further divided into subclasses depending upon either its grain size distribution (coarse-grained soils) or its plasticity (fine-grained soils). All soils are given a two-letter designation descriptive of the soil's primary and secondary classification.

TABLE 2A.7 Unified soil classification chart

Criteria for assigning group symbols and group names using laboratory tests[A]				Soil classification	
				Group symbol	Group name[B]
COARSE-GRAINED SOILS more than 50% retained on No. 200 sieve	Gravels More than 50% of coarse fraction retained on No. 4 sieve	Clean gravels Less than 5% fines[C]	$Cu \geq 4$ and $1 \leq Cc \leq 3$[E]	GW	Well-graded gravel[F]
			$Cu < 4$ and/or $1 > Cc > 3$[E]	GP	Poorly graded gravel[F]
		Gravels with Fines More than 12% fines[C]	Fines classify as ML or MH	GM	Silty gravel[F,G,M]
			Fines classify as CL or CH	GC	Clayey gravel[F,G,H]
	Sands 50% or more of coarse fraction passes No. 4 sieve	Clean sands Less than 5% fines	$Cu \geq 6$ and $1 \leq Cc \leq 3$[E]	SW	Well-graded sand[I]
			$Cu < 6$ and/or $1 > C\sim > 3$"	SP	Poorly graded sand[I]
		Sands with Fines More than 12% fines[D]	Fines classify as ML or MH	SM	Silty sand[G,H,I]
			Fines classify as CL or CH	SC	Clayey sand[G,H,I]
FINE-GRAINED SOILS 50% or more passes the No. 200 sieve	Silts and clays Liquid limit less than 50	inorganic	PI > 7 and plots on or above "A" line[J]	CL	Lean clay[K,L,M]
			PI < 4 or plots below "A" line[J]	ML	Silt[K,L,M]
		organic	$\frac{\text{Liquid limit – oven dried}}{\text{Liquid limit – not dried}} < 0.75$	OL	Organic clay[K,L,M,N] / Organic silt[K,L,M,O]
	Silts and clays Liquid limit 50 or more	inorganic	P1 plots on or above "A" line	CH	Fat clay[K,L,M]
			P1 plots below "A" line	MH	Elastic silt[K,L,M]
		organic	$\frac{\text{Liquid limit – oven dried}}{\text{Liquid limit – not dried}} < 0.75$	OH	Organic clay[K,L,M,P] / Organic silt[K,L,M,O]
HIGHLY ORGANIC SOILS	Primarily organic matter, dark in color, and organic odor			PT	Peat

[A]Based on the material passing the 3-in (75 mm) sieve.

[B]If field sample contained cobbles or boulders, or both, add "with cobbles or boulders, or both" to group name.

[C]Gravels with 5 to 12% fines require dual symbols:
GW-GM well-graded gravel with silt
GW-GC well-graded gravel with clay
GP-GM poorly graded gravel with silt
GP-GC poorly graded gravel with clay.

[D]SandS with 5 to 12% fines require dual symbols:
SW-SM well-graded sand with silt
SW-SC well-graded sand with clay
SP-SM poorly graded sand with silt
SP-SC poorly graded sand with clay.

[E]$Cu = D_{60}/D_{10}$ $\quad Cc = \dfrac{(D_{30})^2}{D_{10} \times D_{60}}$

[F]If soil contains ≥ 15% sand, add "with sand" to group name.

[G]If fines classify as CL-CL, use dual symbol GC-CM, or SC-SM.

[H]If fines are organic, add "with organic fines" to group name.

[I]If soil contains ≥ 15% gravel, add "with gravel" to group name.

[J]If Atterberg limits plot in hatched area, soil is a CL-ML, silty clay.

[K]If soil contains 15 to 29% plus No. 200, add "with sand" or "with gravel," whichever is predominant.

[L]If soil contains ≥ 30% plus No. 200, predominantly sand, add "sandy" to group name.

[M]If soil contains ≥ 30% plus #200, predominantly gravel, add "gravelly" to group name.

[N]P1 ≥ 4 and plots on or above A line.

[O]P1 < 4 or plots below A line.

[P]P1 plots on or above A line.

[Q]P1 plots below A line.

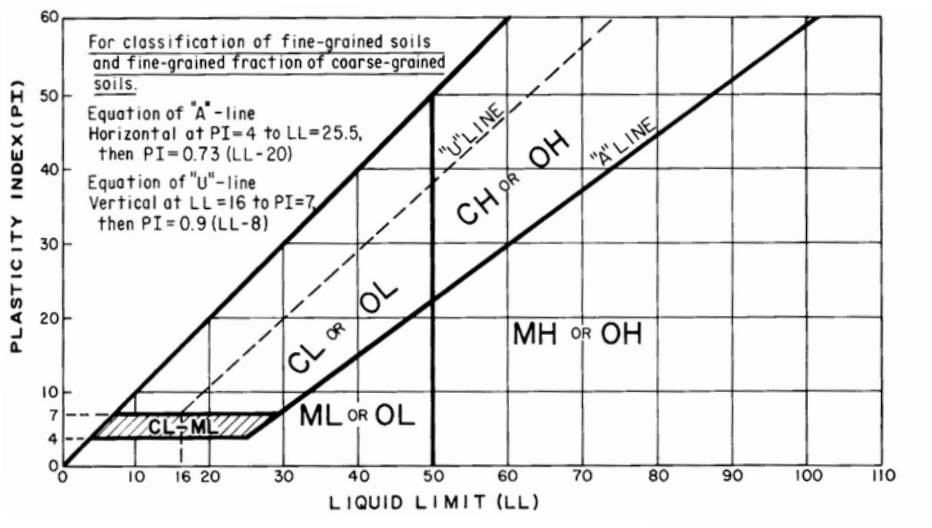

FIGURE 2A.9 Plasticity chart.

Coarse-Grained Soils. Coarse-grained soils are classified as gravel (G) if 50% or more of the coarse fraction is larger than the #4 mesh sieve. The coarse-grained soil is classified as sand (S) if 50% or more of the coarse fraction lies between the #4 and the #200 mesh sieve. Subclasses are well-graded (W), poorly graded (P), silty (M), or clayey (C) based on the amount, distribution, and plasticity of their particles. Details of the classification are given in Table 2A.7.

Fine-Grained Soils. Fine grained soils are classified as either silt (M) or clay (C) depending upon their plasticity as measured by the Atterberg Limits. In order to make this determination, the plasticity chart (Figure 2A.9) is utilized. Once the liquid limit and plasticity indexes are known for the soil, plotting the point on the chart makes the appropriate soil identification. Soils are high plasticity (H) if their liquid limits exceed 50. Soils are low plasticity (L) if their liquid limit is less than 50. The A line separates the clays from the silts and the organic soils. Soils whose liquid limit–plasticity indexes plot above the A line are classified as clays, whereas soils whose liquid limit–plasticity indexes plot below the A line are classified as silts. Organic soils that plot below the A line have visible organic material.

2A.4 WATER FLOW IN SOILS

Many geotechnical engineering problems involve the flow of water through soils. The study of water flow through soils has received much attention due to its importance in seepage and soil consolidation problems. Chemical transport through soils is receiving much more attention due to increased interest in groundwater pollution, waste disposal and storage, and so on.

2A.4.1 Basic Principles of One-Dimensional Fluid Flow in Soils

2A.4.1.1 Darcy's Law

Water flow is related to the corresponding driving forces according to Darcy's law:

$$\text{Water Flow}: q = kiA \tag{2A.23}$$

where q = flow rate (flux) of water

i = hydraulic gradient
k = hydraulic conductivity
A = cross-sectional area of flow

Two general assumptions govern the analysis of fluid flow through soil and rock. The first is that all of the voids are interconnected. The second is that water can flow through even the densest of natural soils. Although the second assumption appears to be valid, it is generally accepted that not all of the void spaces provide passageways for pore fluids.

Darcy's law can be presented as follows for the condition of Figure 2A.10:

$$Q = kiA\Delta t \tag{2A.24}$$

where Q = quantity of flow (volumetric fluid flux, volume units)
i = a forcing function (gradient)
k = fluid conductivity, a coefficient of proportionality related to the properties of the flow medium and the fluid (often called permeability or, more correctly, hydraulic conductivity).
A = cross-sectional area of flow
Δt = time length of flow duration.

Referring to Figure 2A.10, we get

$$q = \frac{Q}{\Delta t} = k\left[\frac{(h_A - h_B)}{L}\right]A = -kiA \tag{2A-25}$$

where h_A = the upstream head = $(h_p + h_z)_A$
h_B = the downstream head = $(h_p + h_z)_B$
h_p = pressure head
h_z = elevation head
L = the length of flow
q = specific fluid flux (flow rate)

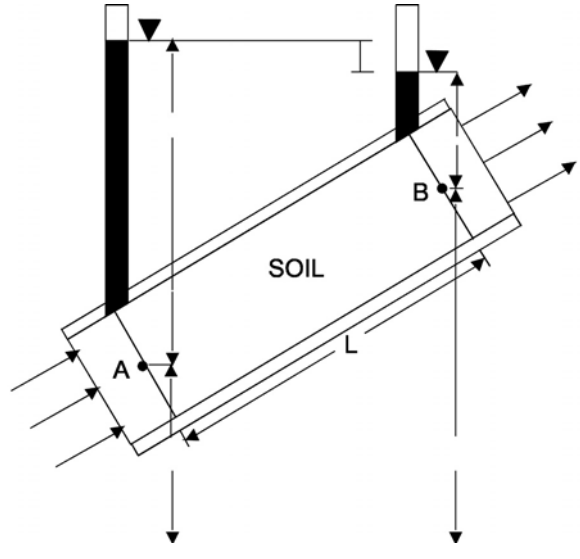

FIGURE 2A.10 Darcy's law.

2A.4.1.2 Flow Velocity

Since flow can only occur through the soil voids,

$$q = VA = v_s A_v \tag{2A.26}$$

where v = approach, apparent or superficial velocity
$= q/A = ki$
v_s = seepage velocity through soil (assumed to be in a straight line)
A = total cross-sectional area of soil volume
A_v = volume of soil voids

$$v_s = v\left[\frac{A}{A_v}\right]\left[\frac{L}{L}\right] = v\left[\frac{V}{V_v}\right] = \frac{v}{n_e} \tag{2A.27}$$

$$v_s = \frac{ki}{n_e} \tag{2A.28}$$

n_e = effective porosity of the soil (pores available for flow)

2A.4.2 Determination of Permeability

2A.4.2.1 Laboratory Methods

It is obvious that the hydraulic conductivity of a soil is, in many cases, the controlling factor in subsurface migration of hazardous wastes. Estimates of contaminant flow quantities and patterns can only be as accurate as the values of hydraulic conductivity used to make them. Subsurface fluid flow may occur under either partially saturated or fully saturated conditions. Numerous methods are available for measurement of hydraulic conductivity of soils either in situ or in the laboratory.

Soils are generally nonhomogeneous and anisotropic. Fine-grained (clay) soils are often stratified, and contain root holes, fissures, and cracks. Therefore, it is desirable to test as large a volume of soil as possible. This usually means that testing should be done in the field. Field methods can usually provide more representative values than laboratory methods because they test a larger volume of material, thus integrating the effects of macrostructure and heterogeneities. However, there are many difficulties in controlling the boundary conditions of field tests.

The most common laboratory methods of measuring the coefficient of hydraulic conductivity in the laboratory are the constant head test and the falling head test.

Constant Head Tests. In the constant head test, the hydraulic gradient, i, is maintained constant at h_w/L (Figure 2A.11). From Darcy's law,

$$k = \frac{q}{iA} = \frac{QL}{(\Delta thA)} \tag{2A.29}$$

where q = specific fluid flow (flow rate)
Q = flow volume in elapsed time, t
L = Length of soil specimen
h = head of water
A = Cross-sectional area of specimen
Δt = elapsed time of test

The main advantages of the constant head test are the simplicity of interpretation of the data and the fact that the use of a constant head minimizes confusion due to changing volume of air bubbles when the soil is not saturated.

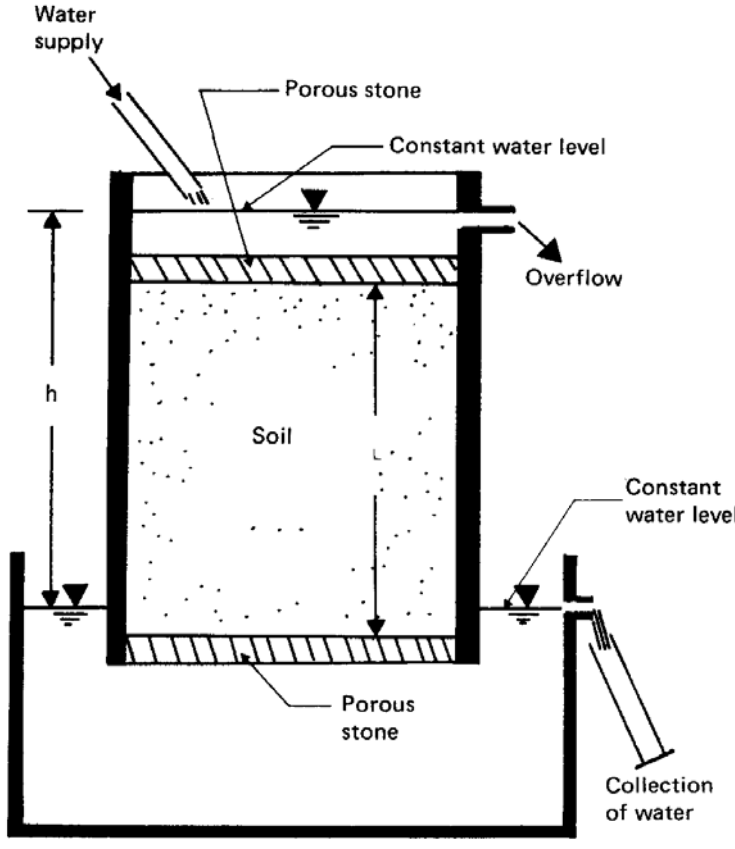

FIGURE 2A.11 Constant head test.

Falling Head Test. In this test,

$$q = a\frac{dh}{dt} \tag{2A.30}$$

where a = the cross sectional area of the burette (Fig. 2A.12). Therefore

$$k = \left[\frac{al}{At}\right]\log_e\left[\frac{h_1}{h_2}\right] \tag{2A.31}$$

The main advantage of this procedure is that small flows are easily measured using the burette. The observation time may be long, in which case corrections for water losses due to evaporation or leakage may be needed.

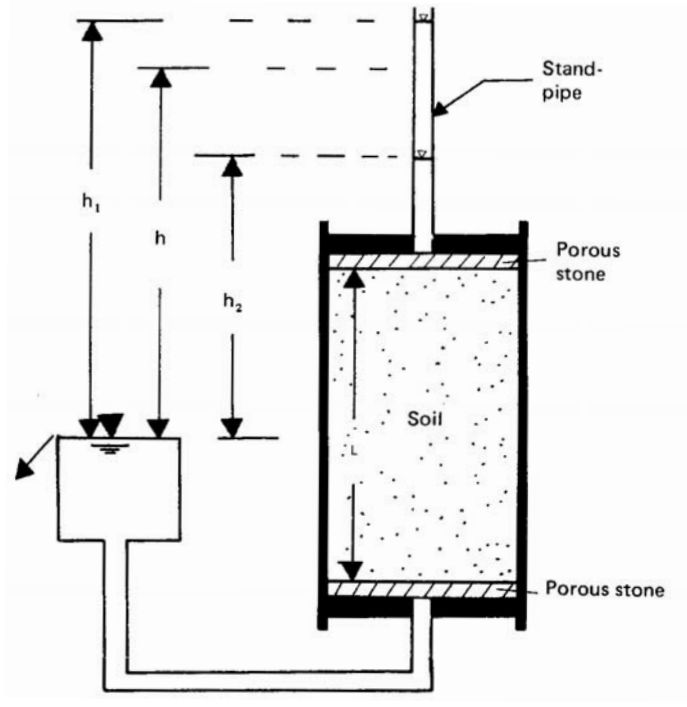

FIGURE 2A.12 Schematic of falling head permeability test.

Triaxial Flexible Wall Permeability Tests. Two techniques are used to confine the soil sample during either the constant or falling head tests: rigid wall confining ring or a flexible membrane.

A flexible wall confined specimen placed in a triaxial permeameter allows us to:[7]

1. Back-pressure saturate
2. Reapply isotropic stresses to simulate field conditions
3. Insure against short-circuiting of permeant
4. Measure independently soil sample volume change

Sources of Error. The following are sources of error in testing:

1. Use of nonrepresentative samples (the overriding source of error)
2. Voids formed during sample preparation
3. Smear zones
4. Alteration in clay chemistry
5. Air in sample
6. Growth of microorganisms
7. Menisci problems in capillary tubes
8. Temperature
9. Volume change due to stress change

2A.4.2.2 Field Methods

The use of field methods for the measurement of hydraulic conductivity had at least two advantages over laboratory techniques: 1) less disturbance of soil, and 2) larger, more representative volume of soil can be tested. The disadvantages of field methods, which are, of course, the advantages of laboratory tests are: 1) less expensive, 2) can saturate the soil fully, 3) can vary the stress, and 4) can test with waste liquids.

The hydraulic conductivity of in situ field soil is usually measured by monitoring the rate of fluid flow into or out of a boring. The coefficient of permeability is then calculated by any one of several available formulas. Heads may vary or be kept constant. Both pump-in and pump-out tests are used.

Auger Method. This method involves the drilling of a hole below the water table, pumping the water in the hole down, and measuring the rate that the water refills the hole (recovery). The coefficient of hydraulic conductivity is calculated using:

$$k = \left[\frac{\pi^2}{16}\right]\left[\frac{r}{Sd}\right]\left[\frac{\Delta h}{\Delta t}\right] \tag{2A.32}$$

where k = hydraulic conductivity
r = radius of the boring
S = Shape factor
d = depth of the bottom of the hole below the water table
h = height of water in the hole
t = time elapsed since the cessation of pumping

This equation is limited to an incompressible soil, a hole drilled to an impervious base, and no drawdown of the water table. Shape factors are given in Fig. 2.13.

Tests Using Cased Holes. In these tests, casings are inserted in the bore holes to the depths where the permeability is to be measured. The coefficient of hydraulic conductivity is calculated by:

$$k = \frac{q}{5.5rh} \tag{2A.33}$$

where r = inside radius of the casing
h = differential head of water
q = rate of supply of water to maintain constant head

Pumping From Wells. The coefficient of hydraulic conductivity can be determined by pumping from a well at a constant rate and observing the steady-state water table in nearby observation wells.

$$q = k\left[\frac{dh}{d}r\right]2\pi rh \tag{2A.34}$$

Solving:

$$k = \left[\frac{(2.303q)}{\pi(h_2^2 - h_1^2)}\right]\log\left[\frac{r_2}{r_1}\right] \tag{2A.35}$$

The equation above has been developed on the assumption that he well fully penetrates the permeable layer.

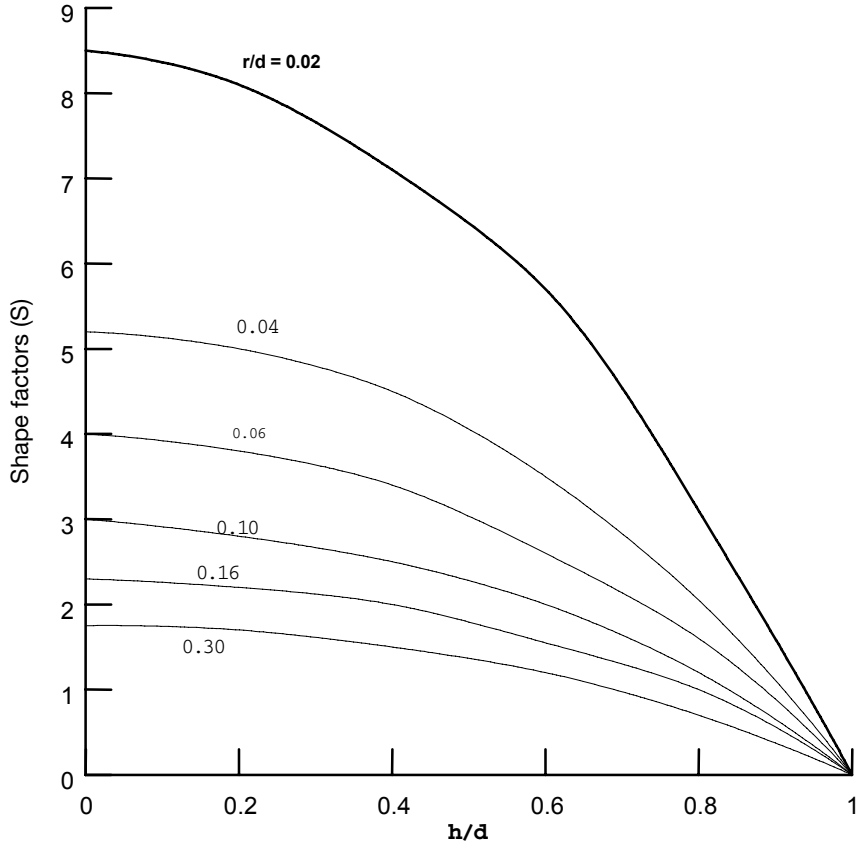

FIGURE 2A.13 Shape factors for auger method.

Tests on Compacted Clay Fills

Sealed Double-Ring Infiltrometer Test. The sealed double-ring infiltrometer (SDRI) is a device designed for making determinations of hydraulic conductivities in the range of 10^{-7} cm/sec to 10^{-10} cm/sec. It is comprised of two concentric rings. To facilitate installation, the ring shape is rectangular rather than circular. Seepage interior to the inner ring is used for the determination of hydraulic conductivity. Water in the annular space between the inner and outer rings prevents lateral seepage from the soil column underlying the inner ring. Although a uniform hydraulic head is maintained over the entire test area, the inner ring is sealed to eliminate effects of evaporation. Fig. 2A.14 shows a schematic of the SDRI installation.

Tensiometers are used to track the wetting front during the test. A tensiometer is a tube with a porous cup at one end and a vacuum gage at the other. First, a hole is augered to the desired depth in the material to be monitored. After being filled with water and ensuring that the porous tip is saturated, the tensiometer is placed in the auger hole. The annular space is then back filled in compacted layers with the soil originally removed from the hole. The tensiometer is then allowed to come into equilibrium with the surrounding soil. Because the surrounding soil is unsaturated and the porous cup is in hydraulic contact with the soil, a vacuum develops in the tensiometer and can be read by the gage

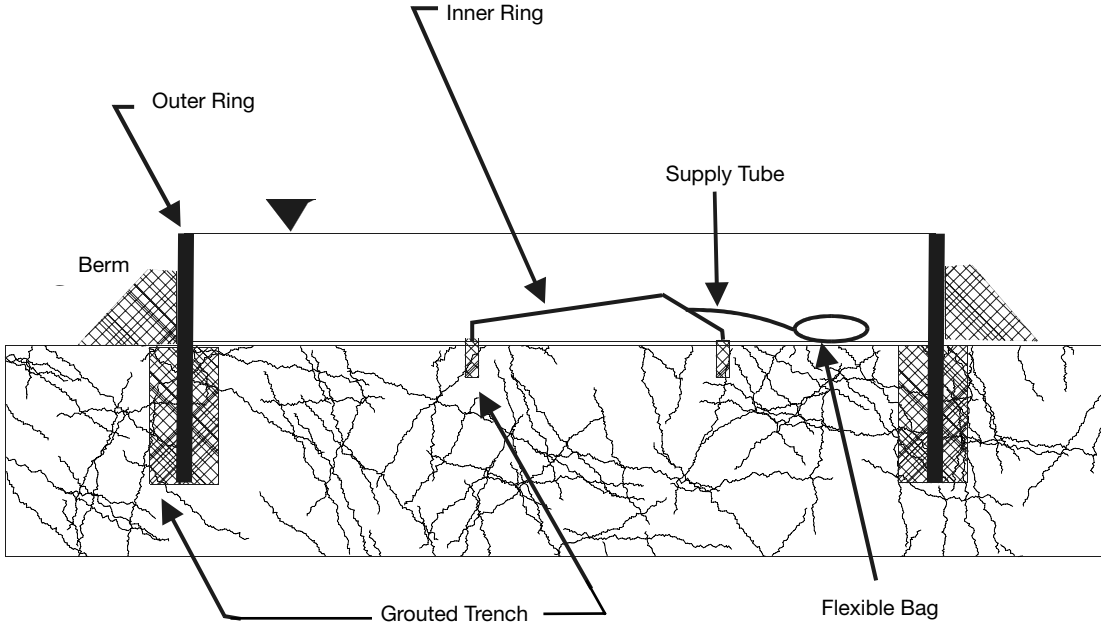

FIGURE 2A.14 Schematic of sealed double ring infiltrometer.

at the top. As the wetting front passes, the pressure will go to zero. Typically, nine tensiometers are installed in the soil in the annular space between the inner and outer rings—three each at depths of 15 cm, 30 cm, and 45 cm. The time at which the wetting front passes each tensiometer is recorded.

Prior to commencing the test, water is placed into the inner ring. The outer ring is filled to a depth of about 280 mm (at least 100 mm over the apex of the dome of the inner ring). This depth is maintained within 25 mm throughout the test and a record of the volume of water added is maintained. A clear flexible bag with a capacity of 1000 ml to 3000 ml (such as an intravenous bag available from medical supply houses) is used to measure the volumetric rate of seepage from the inner ring. It is filled with water, weighed, and attached to the inlet tube. Periodically during the test, the bag is removed and weighed. The record of bag weight change with time is used to compute the infiltration rate.

The test is complete when the infiltration rate becomes constant or when it becomes less than some predetermined value. At this time, the tubing is disconnected from the inner ring, water is drained from the rings, and grout is removed from around the rings to allow the rings to be extracted. The soil in the test area circumscribed by the inner ring is then sampled for a soil moisture profile determination.

The actual determination of hydraulic conductivity entails straightforward application of Darcy's Law. Vertical percolation rate (seepage velocity) can be calculated as the volumetric flow rate divided by the area of exposed soil surface circumscribed by the inner ring. Volumetric flow rate is the mass change over a known period of time, as determined from weight measurements in the bag divided by the density of water:

$$q = \frac{\Delta M}{\Delta t} \cdot \frac{1}{\rho} \tag{2A.36}$$

where q = volumetric flow rate (cm^3/sec)
ΔM = change in mass (gm)
Δt = incremental time over which ΔM is observed (sec)
ρ = density of water (gm/cm^3)

It then follows that the seepage velocity can be computed as

$$v_s = \frac{Q}{D_i^2} \tag{2A.37}$$

where v_s = seepage velocity (cm/sec)
D_i = length of side of inner ring (cm)

The hydraulic gradient is

$$i = \frac{H + L_f h_{we}}{L_f} \tag{2A.38}$$

where H = depth of ponding in the SDRI (cm)
L_f = distance from wetting front to the soil surface (cm)
h_{we} = water-entry suction head (cm), a negative number

There is no universally accepted way of determining h_{we} under field conditions. Therefore, it is usually assumed to be zero.

By rearranging the common expression for Darcy's Law, hydraulic conductivity, k, can be calculated as

$$k = \frac{v_s}{i} = \frac{v_s}{\left(\frac{H + L_f}{L_f}\right)} \tag{2A.39}$$

where k = hydraulic conductivity (cm/sec)

Boutwell Two-Stage Borehole Test. Boutwell developed a two-stage hydraulic conductivity test. The apparatus is shown schematically in Fig. 2A.15. The device is installed by drilling a hole to depth Z. The depth Z must be at least five times larger than D to avoid ambiguities in the interpretation of test results. Furthermore, the depth from the base of the borehole to the bottom of the liner should never be less than about $5D$ for the same reason. After the hole is drilled, a casing is placed inside the hole and the annular space between the casing and borehole is sealed with grout. A cap is placed on the permeameter and a reservoir is used to fill the casing and the standpipe. Once the permeameter has been assembled and filled with water, the Stage I tests are started. The elevation of zero porewater pressure in the soil is assumed to be at the base of the casing such that the head driving the flow is H, as shown in Fig. 2A.15.

A series of falling-head tests are performed, and the hydraulic conductivity from Stage I (k_1) is computed as follows:

$$k_1 = \frac{\pi d^2}{11 D \Delta t} \ln\left(\frac{H_1}{H_2}\right) \tag{2A.40}$$

The values of k_1 are plotted as a function of time until steady conditions are reached. This typically takes from a few days to as much as 2 to 3 weeks. The steady-state value of k_1 is used for later calculations. Next, the top of the permeameter is removed and the hole is deepened with an auger or by pushing in a thin-walled sampling tube. The ratio of length to diameter (L/D) in the uncased zone (Fig. 2A.15) should be between 1.0 and 1.5. The permeameter is reassembled and a series of falling-

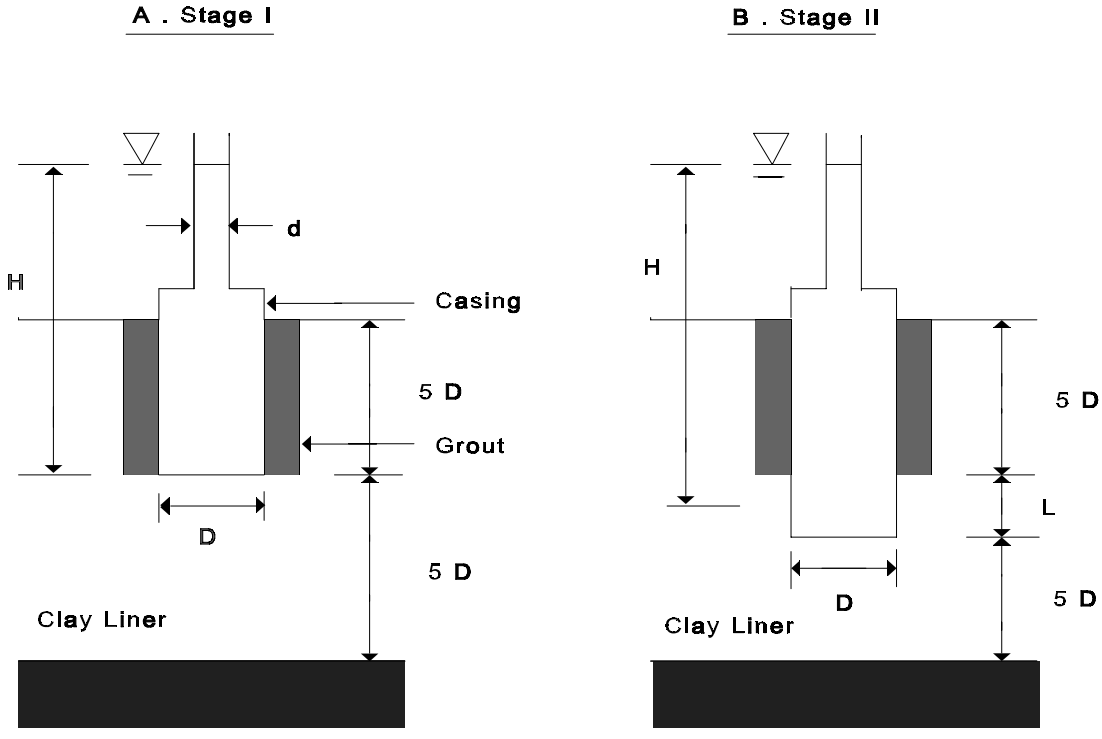

FIGURE 2A.15 Boutwell two-stage hydraulic conductivity test.

head tests are again performed. The head loss (H) is assumed to be as shown in Fig. 2A.15. The hydraulic conductivity from Stage II (k_2) is calculated as follows:

$$k_2 = \left[\frac{A}{B}\right] \ln\left(\frac{H_1}{H_2}\right) \tag{2A.41}$$

where

$$A = d^2\left\{\ln\left[\left(\frac{L}{D}\right) + \left(1 + \left(\frac{L}{D}\right)^2\right)\right]^{0.5}\right\} \tag{2A.42}$$

$$B = 8D\left(\frac{L}{D}\right)(dt)\left\{1.0 - 0.562\exp\left[-1.57\left(\frac{L}{D}\right)\right]\right\} \tag{2A.43}$$

The values of k_2 are plotted as a function of time until k_2 ceases to change significantly. Next, arbitrary values of m are selected, where m is defined as

$$m = \left(\frac{k_h}{k_v}\right)^{0.5} \tag{2A.44}$$

k_h and k_v are the hydraulic conductivities in the horizontal and vertical directions, respectively. The corresponding values of k_2/k_1 are calculated from the expression

$$\left(\frac{k_2}{k_1}\right) = \frac{m \ln\left[\left(\frac{L}{D}\right) + \left(1 + \left(\frac{L}{D}\right)^2\right)\right]^{0.5}}{\ln\left[\left(\frac{mL}{D}\right) + \left(1 + \left(\frac{mL}{D}\right)^2\right)^{0.5}\right]} \tag{2A.45}$$

Typically, values of m ranging from 1 to as much as 10 might be used to compute k_2/k_1. The resulting data are plotted as shown in Fig. 2A.16 for $L/D = 1.0$ and $L/D = 1.5$, and a smooth curve is fitted visually through the data for each L/D ratio. The plot of k_2/k_1 versus m is then entered with the actual value of k_2/k_1 as determined from equations 2A.44 and 2A.45 on the basis of data collected during Stage I and Stage II tests. The actual value of m that corresponds to the actual value of k_2/k_1 is found. The hydraulic conductivities in the vertical and horizontal directions are computed as follows:

$$k_h = mk_1 \tag{2A.46}$$

$$k_v = \left(\frac{1}{m}\right)k_1 \tag{2A.47}$$

The assumptions that were made are that the soil is homogeneous, pore water pressure in the surrounding soil is zero at the base of the permeameter, the soil that is permeated is sufficiently far removed from the boundaries of the liner that the test results are unaffected by boundary conditions, the degree of saturation of soil through which the water flows is uniform, and that soil suction is negligible.

The advantages of borehole tests are that the devices are relatively easy to install, they can be installed at great depth, the cost is relatively low, the hydraulic conductivity in both the vertical and horizontal directions can be measured, and relatively low hydraulic conductivities (10^{-9} cm/sec) can be measured. The disadvantages are that the effects of incomplete and variable saturation are un-

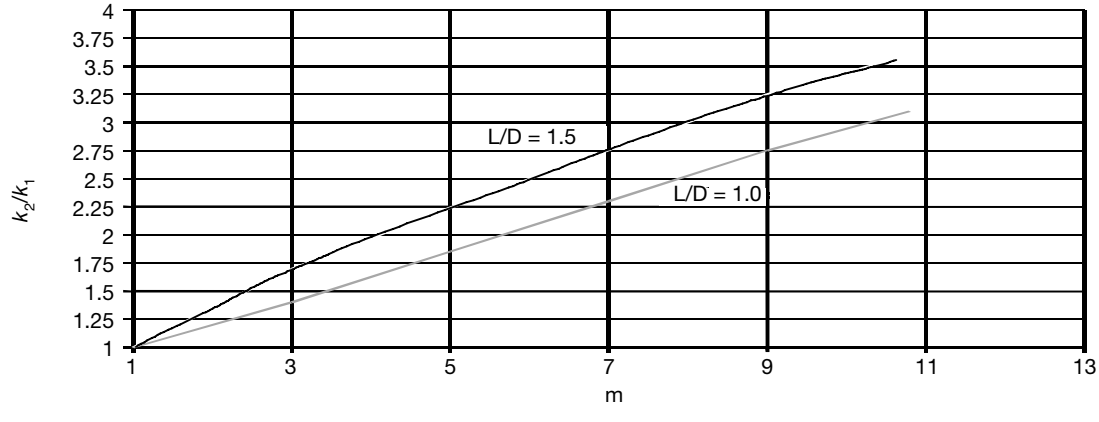

FIGURE 2A.16 k_2/k_1 versus m.

known, the influence of soil suction upon the results is ill defined, the test cannot be used near the top or bottom of a liner, and the volume of soil that is permeated is relatively small.

2A.5 GEOSTATIC STRESSES IN SOIL

The three phases of soil (solid, water, and gas) will react differently to applied stresses and thus a relationship between the phases must be established. The solid particles and water are relatively incompressible and the gaseous phase is highly compressible. The following definitions and relationship between the various phases have been proposed by Terzaghi.

2A.5.1 Total Stresses

Total stress, σ, is the stress acting at a point in a soil mass with a horizontal top surface. The total stress is computed as the total weight of a column of unit area above the point, i.e.,

$$\sigma = \gamma z \tag{2A.48}$$

2A.5.2 Pore Stresses

The pore or neutral stress (u_w) is the stress within the water voids. Since this stress is hydrostatic, it acts equally in all directions. Under no flow conditions (static),

$$u_w = \gamma_w h_w \tag{2A.49}$$

where γ_w = the unit weight of water (9.8 kN/M^3 = 62.4 lbs/ft^3)
h_w = head of water

2A.5.3 Effective Stresses

The intergranular force acting between points of contact of the solid constituents per unit area is termed the effective stress ($\overline{\sigma}$). Effective stress cannot be measured but can be calculated from the general relationship for saturated soils:

$$\overline{\sigma} = \sigma - u \tag{2A.50}$$

Effective stress, not total stress, governs the shear and compressibility behavior of soils.

2A.6 DISTRIBUTION OF APPLIED STRESSES IN SOIL

The stress in a soil mass due to an applied load can most easily be computed from elastic theory. The soil mass is generally assumed to be semi-infinite, homogeneous, and isotropic.

2A.6.1 Point Load

Boussinesq[8] published a relationship for the stress at any point with coordinates (x,y,z) beneath the location of a point load on the surface of the mass in 1885. His equation was:

$$\sigma_z = \frac{3P}{2\pi} \frac{z^3}{(x^2 + y^2 + z^2)^{5/2}}$$

if $x^2 + y^2 + z^2 = R^2$ (2A.51)

$$\sigma_z = \frac{3P}{2\pi} \frac{z^3}{R^5}$$

If $r^2 = x^2 + y^2$

$$\sigma_z = \frac{P}{z^2} \frac{3}{2\pi} \left[\frac{1}{\left(\frac{r}{z}\right)^2 + 1} \right]^{5/2}$$

or $\sigma_z = \frac{P}{z^2} I$ (2A.52)

where I = influence factor = $f(r/z)$

If equation 2A.52 is plotted versus depth z for $r = 0$ (center line), Fig. 2A.17 results. As can be seen, the stress decreases rapidly as the depth beneath the point of load application increases. If

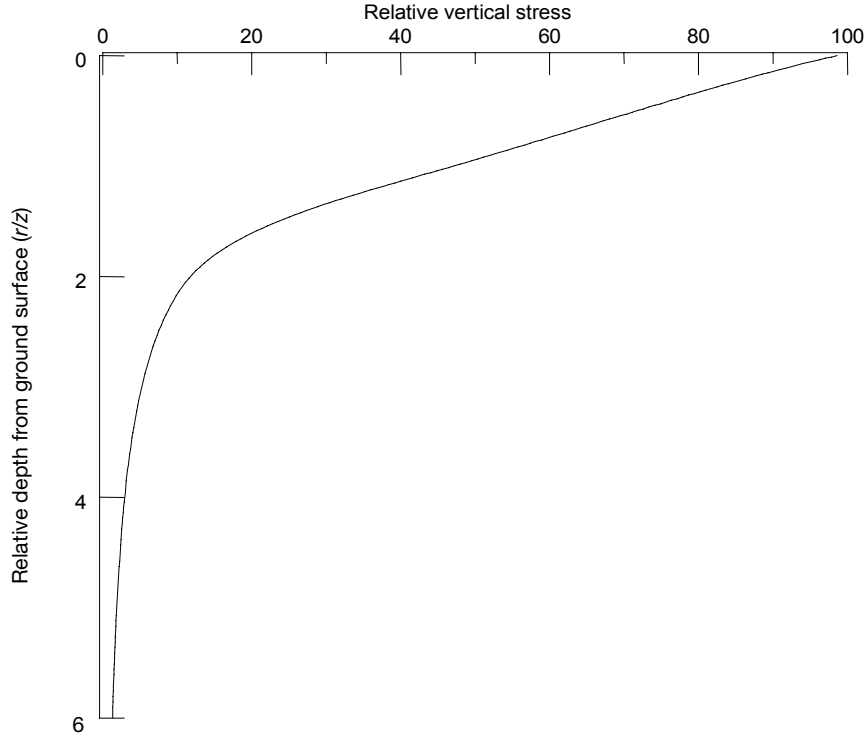

FIGURE 2A.17 Vertical stress versus depth.

equation 2A.52 is plotted versus r for a constant depth z, Fig. 2A.18 results. The stress decreases rapidly as the distance from the axis of the load increases.

2A.6.2 Uniformly Loaded Strip

Equation 2A.52 can be used to determine the stress beneath a flexible strip load of width B (Fig. 2A.19). Using the terms defined in Fig. 2A.19, the following equation can be developed:

$$\sigma_v = \frac{q}{\pi}[\beta + \sin\beta\cos(\beta + 2\sigma)] \tag{2A.53}$$

where $q = P/A$ = load/unit area

Table 2A.8 shows the variation of σ/q with $2z/B$ for various values of $2x/B$.

2A.6.3 Uniformly Loaded Circular Area

The Boussinesq point load equation can be used to develop an expression for the vertical stress below the center of a uniformly loaded flexible circular area:

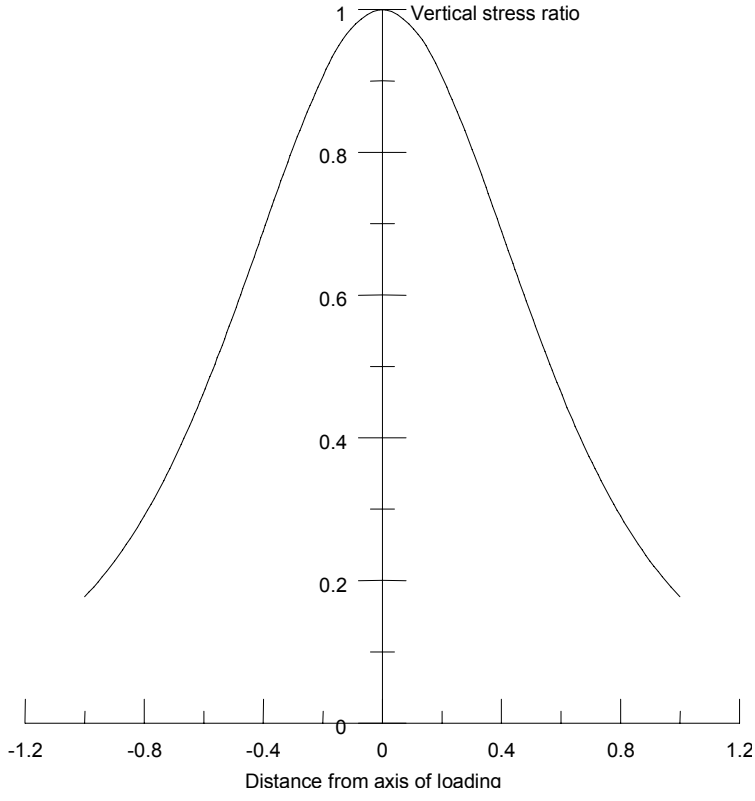

FIGURE 2A.18 Vertical stress versus r.

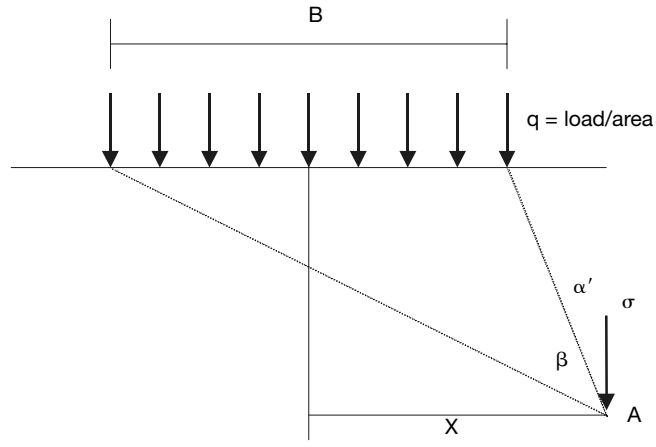

FIGURE 2A.19 Vertical stress due to a flexible strip load.

TABLE 2A.9 Variation of σ/q with $2z/B$ and $2x/B$

$2x/B$	$2z/B$	σ/q	$2x/B$	$2z/B$	σ/q
0	0.0	1.0000	1.5	1.0	0.2488
	0.5	0.9594		1.5	0.2704
	1.0	0.8183		2.0	0.2876
	1.5	0.6678		2.5	0.2851
	2.0	0.5508	2.0	0.25	0.0027
	2.5	0.4617		0.5	0.0194
	3.0	0.3954		1.0	0.0776
	3.5	0.3457		1.5	0.1458
	4.0	0.3050		2.0	0.1847
0.5	0.0	1.0000		2.5	0.2045
	0.25	0.9787	2.5	0.5	0.0068
	0.5	0.9028		1.0	0.0357
	1.0	0.7352		1.5	0.0771
	1.5	0.6078		2.0	0.1139
	2.0	0.5107		2.5	0.1409
	2.5	0.4372	3.0	0.5	0.0026
1.0	0.25	0.4996		1.0	0.0171
	0.5	0.4969		1.5	0.0427
	1.0	0.4797		2.0	0.0705
	1.5	0.4480		2.5	0.0952
	2.0	0.4095		3.0	0.1139
	2.5	0.3701			
1.5	0.25	0.0177			
	0.5	0.0892			

$$\sigma_v = q\left[1 - \frac{1}{\left[\left(\frac{R}{z}\right)^2 + 1\right]}\right]^{3/2} = qI \tag{2A.54}$$

where R = radius of loaded area
I = influence factor

Table 2A.9 gives I for various values of z/R.

2A.6.4 Uniformly Loaded Rectangular Area

The vertical stress below a corner of a flexible rectangular loaded of width B and length L can be computed from

$$\sigma_v = qI_3 \tag{2A.55}$$

where

$$I_3 = \frac{1}{4\pi}\left[\frac{2mn\sqrt{m^2+n^2+1}}{m^2+n^2+m^2n^2+1}\left(\frac{m^2+n^2+2}{m^2+n^2+1}\right)\right] + \frac{1}{4\pi}\left[\tan^{-1}\left(\frac{2mn\sqrt{m^2+n^2+1}}{m^2+n^2-m^2n^2+1}\right)\right]$$

$$m = \frac{B}{z}$$

$$n = \frac{L}{z}$$

The variation of I_3 is shown in Fig. 2A.20. The special case of the stress beneath the center of a square loaded area with side B is given in Table 2A.10.

TABLE 2A.9 I vs z/R for circular loaded area

z/R	I
0.0	1.0
0.02	0.9999
0.05	0.9998
0.10	0.9990
0.2	0.9925
0.4	0.9488
0.5	0.9106
0.8	0.7562
1.0	0.6765
1.5	0.4240
2.0	0.2845
2.5	0.1996
3.0	0.1436
4.0	0.0869
5.0	0.0571

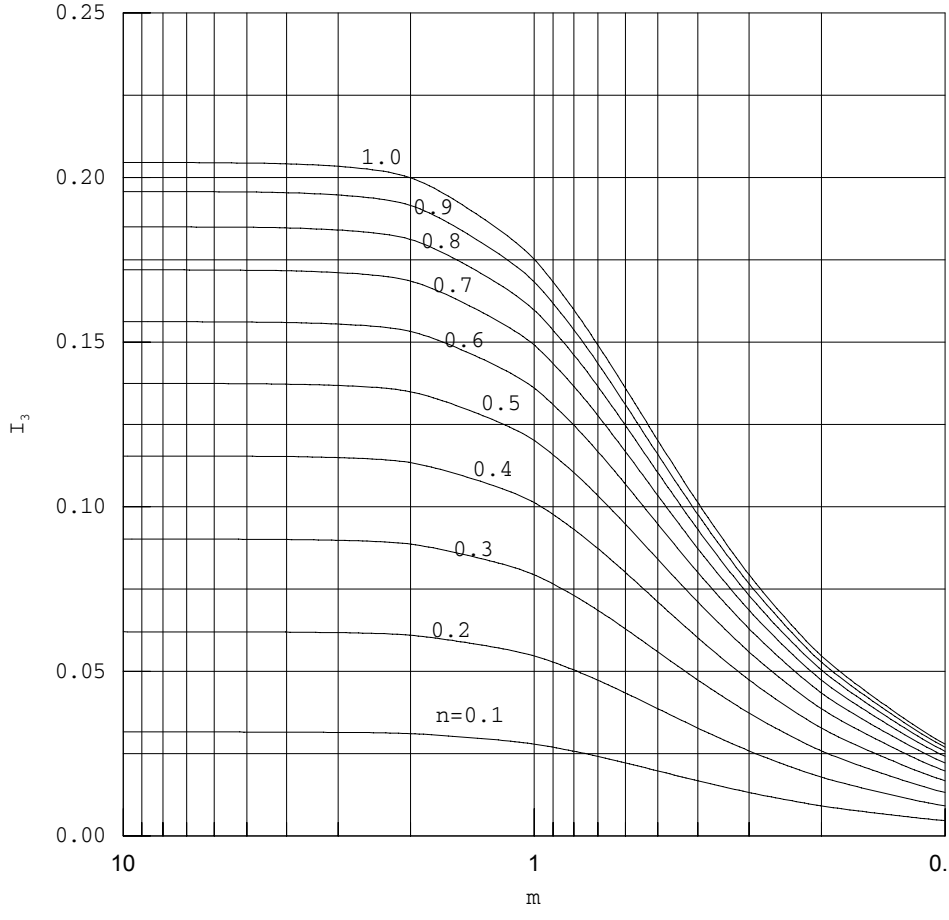

FIGURE 2A.20 Variation of I_3 with m and n.

TABLE 2A.10 Influence factors for stress beneath the center of a square load

B/z	I	B/z	I
0.0	1.0000	2.4	0.7832
20.0	0.9992	2.0	0.7008
16.0	0.9984	1.8	0.6476
12.0	0.9968	1.6	0.5844
10.0	0.9944	1.4	0.5108
8.0	0.9892	1.2	0.4276
6.0	0.9756	1.0	0.3360
5.0	0.9604	0.8	0.2410
4.0	0.9300	0.6	0.1494
3.6	0.9096	0.4	0.0716
3.2	0.8812	0.2	0.0188
2.8	0.8408	0.0	0.0000

2A.6.4 Average Stress Influence Chart

The point load equation has been used to compute average stresses beneath a of circular, square and rectangular uniformly loaded footings. The results are presented as Fig. 2A.21. To use this chart enter the chart with the appropriate depth ratio (z/B) with B being the least dimension. Using the curve for the appropriate shape, read the influence factor on the abscissa. The average stress is the product of the influence factor times the applied stress.

2A.7 ONE-DIMENSIONAL CONSOLIDATION

Assume that the soil stratum shown in Fig. 2A.22 has been formed by sedimentation. If we assume that the element of soil is in equilibrium with its overburden, then the effective overburden

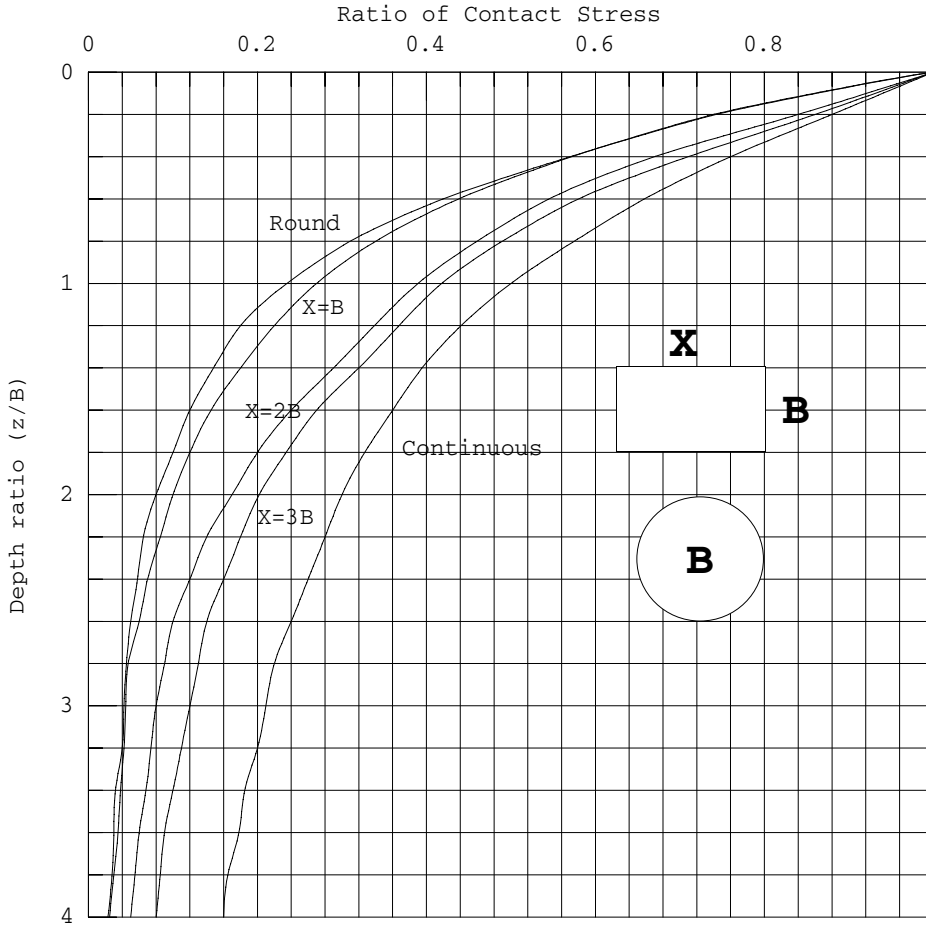

FIGURE 2A.21 Average stress beneath a loaded area.

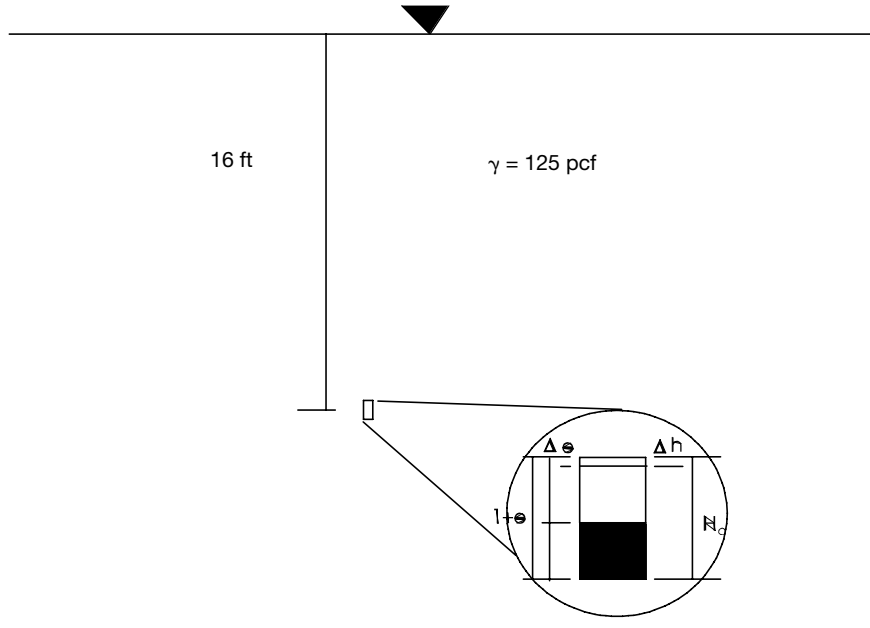

FIGURE 2A.22 Consolidation of a soil element.

$$\frac{\Delta e}{1+e} = \frac{\Delta h}{H_0}$$

$$\Delta h = \frac{H_0 \Delta e}{1+e} \tag{2A.56}$$

stress on that soil element is $\overline{\sigma} = \gamma z = (125 - 62.4)16 = 1000$ psf. In this state, the soil has a void ratio of e ($wG_s = 1.17$) and an element height of H_0. If a very wide fill is placed on top of the soil strata, the stress on the soil element is increased by an amount Δp ($\gamma_{\text{fill}} \cdot h_{\text{fill}}$). This increase in stress causes the void ratio (and the height) of the soil to decrease (settle), as you can see from the figure.

Therefore, if we can determine the relationship between the change in void ratio (Δe) and the applied stress, we can compute the settlement of the soil. This relationship is usually determined from a laboratory one-dimensional consolidation test.

2A.7.1 One-Dimensional Laboratory Consolidation Test

The one-dimensional consolidation test is performed using a disc-shaped sample of soil that is confined around its periphery by a rigid, impervious ring. The specimen is loaded on its flat surfaces through porous stones that allow the water from the soil voids to escape but restrain the soil particles from moving. All deformation occurs parallel to the axis of the specimen (Fig. 2A.23)

2A.7.1.1 Performance of a Consolidation Test

The procedures used in performing one-dimensional consolidation tests vary widely, depending on such factors as soil type, sampling method, and nature of the problem in the field (foundation of

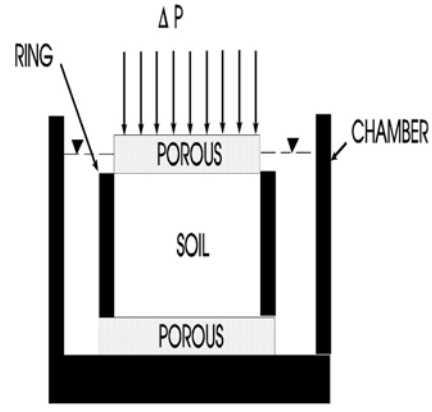

FIGURE 2A.23 Fixed ring consolidometer.

building, embankment, etc.). The procedures recommended in ASTM D2435 are recommended for normal situations.

The soil sample is removed from the sampling tube in such a manner as to minimize further disturbance. A suitable length of soil is removed and is carefully trimmed into the ring. The cell is placed in the loading frame and a seating load is applied, the size of which depends on the strength of the soil. The dial indicator used to measure the axial deformation of the soil is mounted in the frame and an initial reading is taken. The consolidation cell is then filled with water. The applied pressure is adjusted continuously until the soil comes to equilibrium with the pressure at constant volume.

The first increment of consolidation pressure is then applied and the soil begins to consolidate. A series of readings of axial deformation are made at preselected times. The consolidation pressure is maintained constant until consolidation has essentially ceased. The standard load increment duration for each pressure is 24 hours (ASTM D2435 Method A), although shorter or longer times may be used depending on the coefficient of consolidation of the soil and the thickness of the sample. Sufficient time-deformation readings are taken to insure that consolidation is complete. For some soils, a period of more than 24 hours may be required to reach end-of-primary consolidation. Usually, the load increment duration is some multiple of 24 hours and should be the standard duration for *all load intervals*.

When consolidation is essentially complete under the first pressure, the next increment of pressure is applied and the deformation reading taken again. The process is repeated until some preselected maximum consolidation pressure is attained. It is usual practice to double the pressure for each successive increment. Thus, for a typical consolidation test, the sequence of pressures might be 125, 250, 500, 1000, 2000, 4000, 8000, 16000, 32000, and 64000 psf. The highest pressure is controlled by the capacity of the frame, economics, and time limitations, or a variety of other factors.

After the deformation has ceased under the highest load, the loads are removed in a series of decrements such that the pressure is usually reduced by four times for each decrement. The final pressure is usually of the order of 125 psf. When the specimen has equilibrated under the final pressure, the apparatus is dismantled rapidly to prevent the soil from imbibing a significant amount of water after the final pressure has been removed.

2A.7.1.2 Calculation of the Laboratory Consolidation Curve

The results of the consolidation test are normally presented as plots of void ratio, e, versus the logarithm of applied pressure, $\bar{p}$. A plot of the pressure-void ratio curve from the test is shown in Fig.

2A.24. As you can see, the curve is highly nonlinear. If that same data is plotted on a semilogarithmic plot e vs $\log_{10} p$, Fig. 2A.25 results. The e–log p plot has an initially shallow slope that transitions into a steeper slope.

As you can see from the plot, the deformations are relatively small until the load approaches the in situ ($\bar{p}_0$) pressure. When the load exceeds the in situ pressure, the deformation increases dramatically. The pressure where the e–log p curve increases slope is called the *maximum past consolidation pressure* (*preconsolidation pressure,* $\bar{p}_c$) and is the greatest stress that has ever been on the soil. For the case studied here, $\bar{p}_c = 1000$ psf $= \bar{p}_0$). The portion of the e–log p curve from the first load to $\bar{p}_c$ is called the *reload* or *recompression* curve, since the soil is being reloaded to its maximum past value. The portion of the e–log p curve for loads greater than $\bar{p}_c$ is called the *virgin consolidation* curve because each additional load is greater than any load that has ever been on the soil previously. Soils where $\bar{p}_c \approx \bar{p}_0$ are called *normally consolidated soils*.

In some (in fact, in most) cases, $\bar{p}_c \ll \bar{p}_0$. This implies that the soil has been more heavily loaded in its past than it is now. Soils with this stress history are called *overconsolidated soils*. Compared to normally consolidated soils, overconsolidated soils are stiffer and less compressible. As before, that portion of the e–log p curve to the $\bar{p}_c$ is the reloading branch, whereas that portion beyond $\bar{p}_c$ is the virgin consolidation branch.

2A.7.1.3 Reconstruction of the Field Consolidation Curve

The consolidation curve shown in Fig. 2A.25 is assumed to be typical of field consolidation curves. The recompression curves merge smoothly with the virgin consolidation curve and have a region of

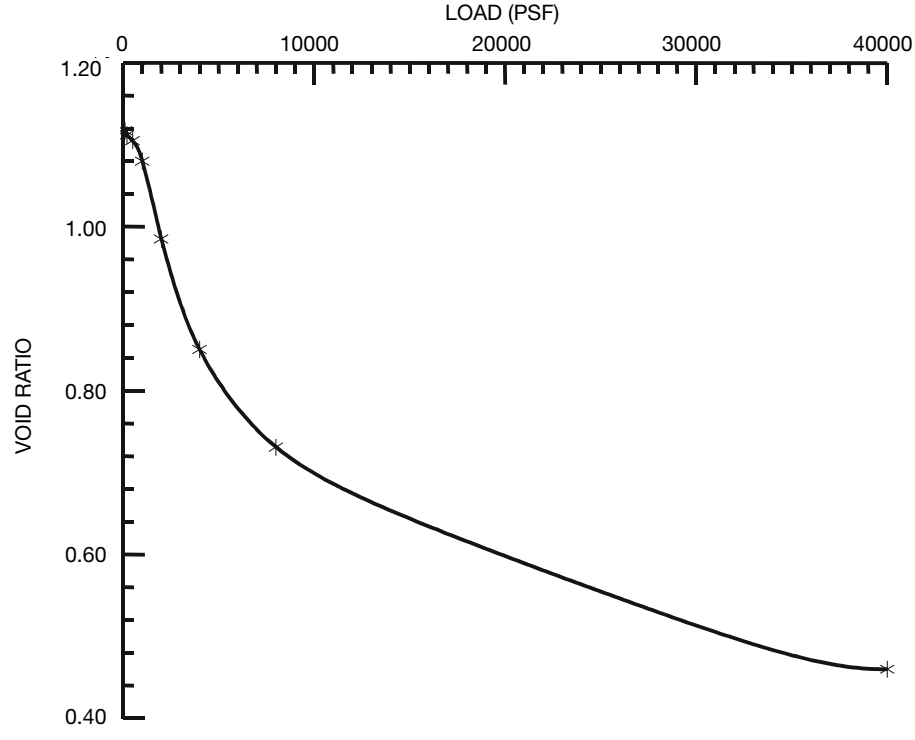

FIGURE 2A.24 e–p plot.

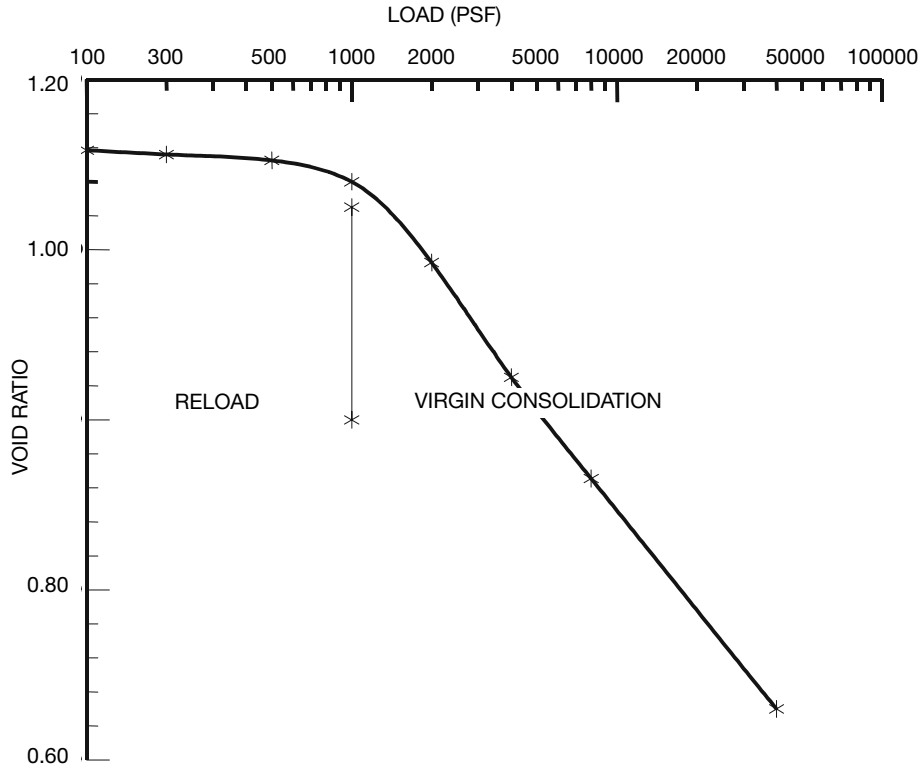

FIGURE 2A.25 e–log p.

sharpest curvature in the vicinity of the maximum previous consolidation pressure, $\bar{p}_c$. Disturbance of soil samples during sampling, transportation, storage, and trimming causes the laboratory curve to be displaced to lower void ratios and to have less pronounced curvature in the vicinity of $\bar{p}_c$.[9,10] A procedure is needed for reconstruction of the field consolidation curve from a slightly disturbed laboratory curve. No exact method for reconstruction of the field curve exists. The available methods are based on laboratory tests and field experience.

The first step is to obtain an estimate of the maximum previous stress under which the soil was consolidated, $\bar{p}_c$. Although several procedures have been proposed, the one suggested by Casagrande[9] seems to be the most satisfactory and most widely used. The procedure is shown in Fig. 2A.26. At the point of sharpest curvature of the laboratory curve, two lines are drawn, one tangent to the laboratory curve and the other horizontal. The angle between these lines is bisected by a third line. The intersection of the bisecting line and the extended laboratory virgin consolidation curve is taken as an approximation of the maximum previous consolidation pressure. If this pressure is approximately equal to the calculated effective overburden pressure in the field, $\bar{p}_0$, then the soil is assumed to be normally consolidated. One point on the field curve is then $e_0, \bar{p}_c$, where e_0 is the initial void ratio of the sample. The field consolidation curve is drawn to pass through the point $e_0, \bar{p}_c$, and to be asymptotic to the laboratory curve at high pressures (Fig. 2A.27).

If the samples used in the laboratory are normally consolidated and have a maximum of disturbance, the $e_0, \bar{p}_0$ point is so near the backwards extension of the laboratory virgin curve that the field

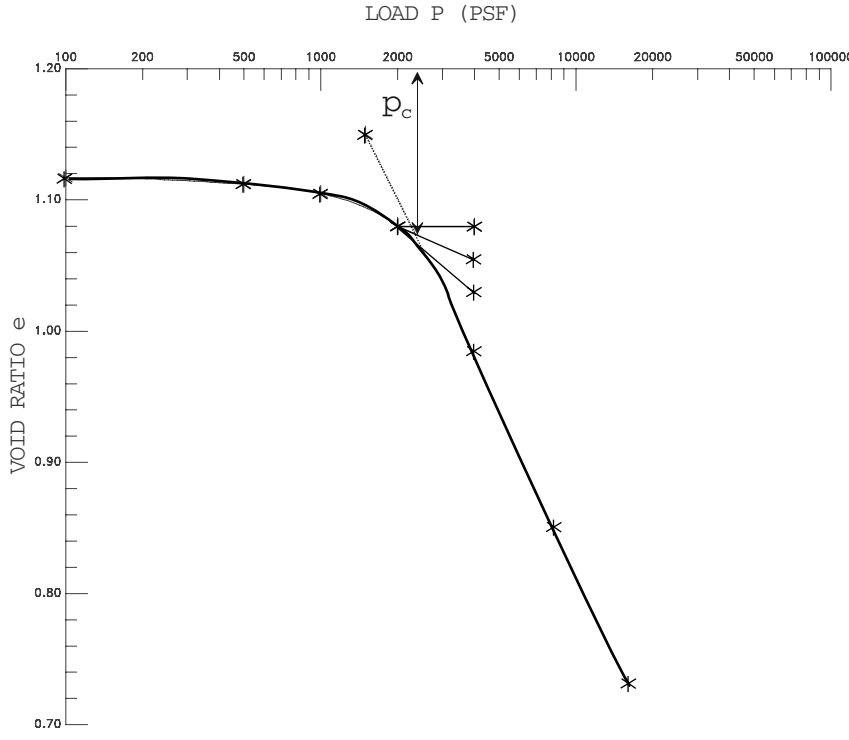

FIGURE 2A.26 Casagrande construction for preconsolidation pressure.

curve can be drawn without use of Casagrande's construction. If the soil is badly disturbed, the laboratory consolidation curve will not have an obvious point of sharpest curvature and no known construction, will give a reasonable approximation of the field curve. The construction, then, is of greatest value for slightly disturbed or overconsolidated specimens.

If Casagrande's construction indicates that p_c exceeds p_0 by a significant amount, then the soil is overconsolidated. The reconstruction of the field curve then is based on the procedure recommended by Schmertmann (1955). A laboratory curve for a sample of highly plastic, overconsolidated, clay is shown in Fig. 2A.27. Casagrande's construction is used to estimate the maximum previous consolidation pressure, the effective overburden pressure in the field is calculated, and the point e_0, $\bar{p}_0$ is plotted. For the moment it will be assumed that the soil is simply overconsolidated, i.e., that it was consolidated to some maximum effective stress in the field and then rebounded directly to the point e_0, $\bar{p}_0$. Furthermore, the field rebound curve is assumed to be parallel to the laboratory rebound curve. Thus, a curve may be drawn parallel to the laboratory rebound curve back from a point on the $\bar{p}_c$ line such that the rebound curve passes through the e_0, $\bar{p}_0$ point. The point on the $\bar{p}_c$ pressure line is then one point on the field virgin consolidation curve. The actual field curve must pass through the point e_0, $\bar{p}_0$, must pass through the pressure $\bar{p}_c$ lower than the "known" point on the field virgin curve, but must remain above the laboratory curve. The reconstructed field curve is drawn in by eye and merged gradually with the laboratory virgin curve (Fig. 2A.27). Schmertmann[11] suggested certain refinements to the method just suggested.

A number of problems arise when attempts are made to apply the foregoing method. First, for many highly overconsolidated soils, the reloading curve of even hand-carved samples appears to be

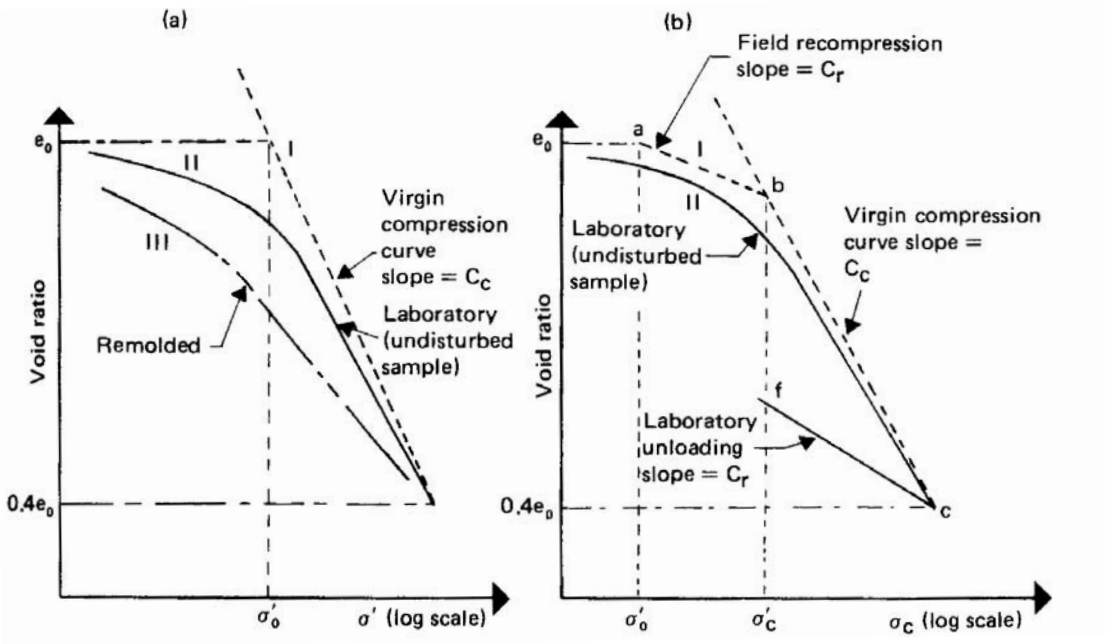

FIGURE 2A.27 Construction of field consolidation curve.

a continuous smooth curve and there is no apparent method for estimating the maximum previous consolidation pressure. Such curves are common for clayey glacial tills. It is also possible that the soil has been rebounded to a pressure much less than the existing overburden pressure and is now on a reloading, rather than rebounding, curve.

Based on the foregoing comments, it seems apparent that reconstruction of the field curve is based largely on the judgment of the soils engineer aided by certain constructions. The uncertainty in estimating the position of the field curve will be reduced if relatively undisturbed samples are used.

2A.7.1.4 Calculation of the Coefficient of Consolidation

The time required for consolidation of a soil can be computed from

$$T = \frac{c_v t}{H_d^2} \tag{2A.57}$$

where T = time Factor (see Table 2A.11)
H_d = maximum drainage distance

For the case of a soil layer loaded very quickly with drainage allowed on both sides, the time–settlement curve can be calculated, provided that the ultimate settlement, S_u, and the coefficient of consolidation, c_v, are known. The ultimate settlement can be calculated from the reconstructed field consolidation curve using the methods discussed previously. The coefficient of consolidation for use in field analyses is also usually estimated from laboratory consolidation tests.

In the laboratory, there is a nearly instantaneous initial settlement, which may be caused by elastic compression of the experimental apparatus, seating of the porous stones against improperly

trimmed faces of the soil specimen, or compression of gas bubbles in the soil. This rapid settlement, termed *initial compression*, obviously cannot be taken into account by the theory. Thus, an adjustment must be made to the laboratory curve to remove the effects of initial compression.

There are two procedures in common use for estimating the appropriate values of S_0 and S_{100}. They are designated Taylor's method[12] and Casagrande's method.[13]

2A.7.1.4.1 Taylor's Method of Finding c_v. When Taylor's method is used, the settlement is plotted versus the square root of time. A square root versus time curve from a one-dimensional consolidation test is shown in Fig. 2A.28.

The corrected initial point for the theoretical curve is found just by extending the linear portion of the laboratory square root of time curve (Fig. 2A.28) back to time zero.

Taylor found that there was no distinct change in the square root of time curve to show where primary and secondary compression merged. In an attempt to find S_{100}, Taylor made the assumption that secondary effects could be ignored of U less than or equal to 90%. Further, he noted that at 90% ultimate consolidation ($U = 90\%$), the abscissa of the laboratory curve would be

$$F\sqrt{t_{90}} = F\left[\frac{H^2}{c_v}\right]^{0.5}(T_{90})^{0.5} \tag{2A.58}$$

where F is just the scale factor originally used to lay out the time scaler on the graph paper. If the linear portion of the square root of time laboratory curve is extended as a straight line to higher values of U, at $U - 90\%$ the abscissa of this straight line is:

$$\left(\frac{9}{5}\right)F\left(\frac{H^2}{c_v}\right)^{0.5}(T_{50})^{0.5} \tag{2A.59}$$

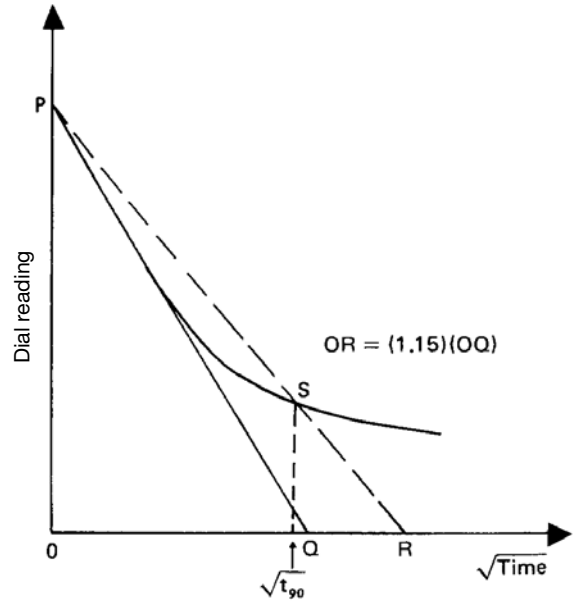

FIGURE 2A.28 Taylor's square root of time plot.

This abscissa was found by linear extrapolation from the point at which $U = 50\%$. But the same abscissa is found if the extrapolation is from some other point on the linear portion of the laboratory curve. At the settlement corresponding to $U = 90\%$, the ratio of the abscissa of the laboratory curve to that of the extended linear curve is

$$\frac{\left[F\left(\frac{H^2}{C_v}\right)^{0.5}(0.848)^{0.5}\right]}{\left[\left(\frac{9}{5}\right)F\left(\frac{H^2}{C_v}\right)^{0.5}(0.197)^{0.5}\right]} \tag{2A.60}$$

Secondary effects are in fact negligible for U less than 90%. At the point $U - 90\%$, $\Delta S_{90} = 0.9\Delta S_{100}$; since ΔS_{90} is known, ΔS_{100} is easily calculated.

It is convenient to select the point at which U is 45% to calculate c_v because the settlement at this point is the average of the known settlements S_0 and S_{90}, thus simplifying the construction used to find the point, and because selection of a point on the linear portion of the laboratory curve ensures that the theoretical and experimental curves will coincide in the region of greatest practical interest. The time factor at 45% consolidation is 0.159 (Table 2A.11). It may be noted that Taylor (1948) recommended use of the $U = 90\%$ point. The coefficient of consolidation is then calculated from:

$$C_v = \frac{0.159H_d^2}{t_{45}} \tag{2A.61}$$

where H_d is the average drainage distance during the consolidation period (half the average total thickness for double drainage) and t_{45} is the time corresponding to $U = 45\%$.

2A.7.1.4.2 Casagrande's Method of Calculating c_v. When Casagrande's method is used, the settlement is plotted versus the logarithm of time. Curves such as the one shown in Fig. 2A.29 (plotted using the same data previously shown in Fig. 2A.28) are typically obtained. An even spacing of points along the curve is obtained by using a geometric progression of times at which the deformations of the specimen are recorded. Typical times are 6, 15, and 30 seconds, 1, 2, 4, 8, 15, and 30 minutes, and 1, 2, 4, 8, and 24 hours, all measured from the instant of load application.

The value of S_0 is again obtained as shown on Fig. 2A.29, based on the parabolic approximation of the early part of the theoretical S–t curve.

TABLE 2A.11 Time Factors

U(%)	T	U(%)	T
10	0.008	55	0.238
15	0.018	60	0.287
20	0.031	65	0.342
25	0.049	70	0.405
30	0.071	75	0.477
35	0.096	80	0.565
40	0.126	85	0.684
45	0.159	60	0.848
50	0.197	95	1.127

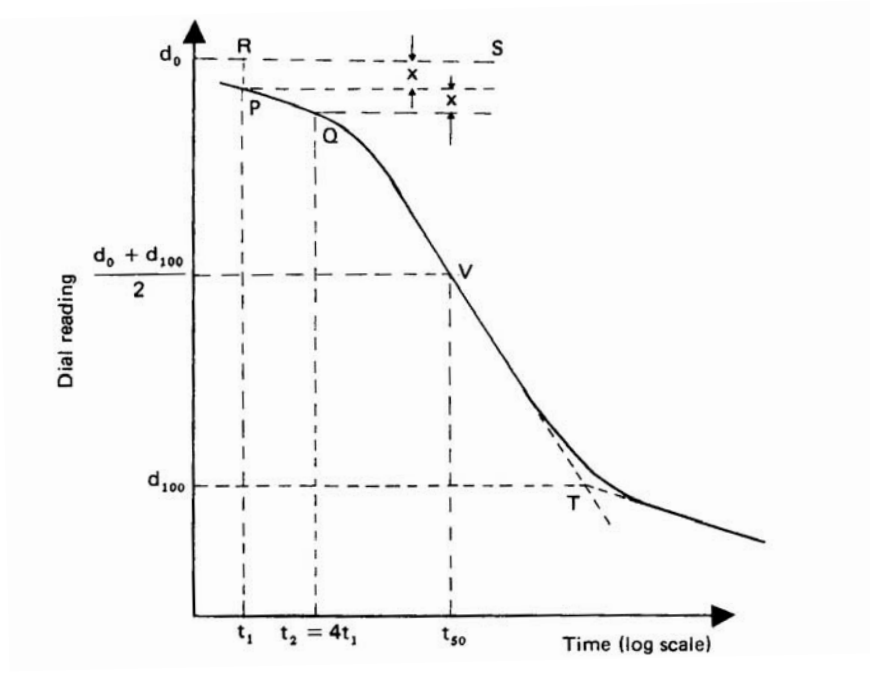

FIGURE 2A.29 Casagrande's log time plot.

$$\Delta S_2 = \Delta S_1 \sqrt{\frac{t_2}{t_1}} \tag{2A.62}$$

If $t_2 = 4t_1$, then, $\Delta S_2 = 2\Delta S_1$ and $S_0 = S_1 - (\Delta S_2 - \Delta S_1$. Because both Casagrande's method and Taylor's method for finding the corrected zero point are based on the assumption that the early part of the S–t curve is a parabola they should yield the same corrected zero point. They differ mainly in the fact that the parabolic part of the curve is clearly visible in the square root plot but is masked in the logarithmic plot. Thus, if Casagrande's method is used, t_2 should be chosen at about t_{50} to maximize the possibility that both points will be on the parabolic part of the curve.

The construction used to locate the maximum theoretical settlement, S_{100}, is shown in Fig. 2A.29. On the semilogarithmic plot, the experimental curves do not become asymptotic to a horizontal line, as required by Terzaghi's theory, but, instead, often become linear, or nearly linear, with a finite slope. The settlement S_{100} is estimated to be the settlement at the intersection of two straight lines, one drawn tangent to the sloping part of the laboratory curve and the other drawn tangent to the laboratory curve at the point of inflection.

To simplify construction and to make the theoretical and experimental curves coincide in the range of greatest field interest, c_v is calculated using t at $U = 50\%$.

It is interesting to note that the two methods give quite different values of S_{100} and thus different values of c_v. Since Taylor's method of finding S_{100} is based on the invalid assumption that secondary effects are negligible prior to 90% consolidation and Casagrande's method has no theoretical justification at all, it is not surprising that they sometimes yield different results.

2A.8 SHEAR STRENGTH OF SOIL

2A.8.1 Introduction

The shear strength of soil depends upon the consolidation pressure, the drainage during shear, the volumetric history (initial relative density of sands or stress history for clays), and other factors such as disturbance, strain rate, stress path, etc.

2A.8.2 Laboratory Tests for Shear Strength of Soil

Numerous types of devices have been developed to measure the shear properties of soil. By far, the most popular and widely used methods are the direct shear, triaxial shear, and unconfined compression devices.

2A.8.2.1 Direct Shear Testing of Soil

A schematic section through a direct shear apparatus is shown in Fig. 2A.30. A vertical or normal stress, σ_n, is applied. The horizontal shear stress, τ, is then increased until failure occurs. If the shear stress is plotted against the horizontal (shear), a curve similar to Fig. 2A.31 results.

Now a *series* of direct shear tests are performed on three different soil samples. However, each test is performed with a different vertical normal stress, $\sigma_n = N/A$ (Fig. 2A.32). The maximum shear stress for each test, τ_f, is called the shear strength.

Plotting the shear strengths from each test against the normal (vertical) stresses, and connecting these failure points results in a failure line, as shown in Fig. 2A.33. This failure line insects the τ axis at c, and is inclined at an angle ϕ to the horizontal. The equation of the failure line (failure envelope) is:

$$\tau_{\max} = s = c + \sigma_n \tan \varphi \tag{2A.63}$$

where $\tau_{\max}$ = shear stress at failure = s, shear strength
σ_n = normal stress on failure plane
φ = angle of internal friction
c = cohesion intercept

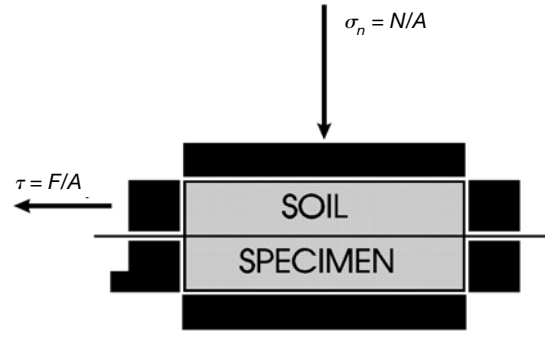

FIGURE 2A.30 Direct shear apparatus.

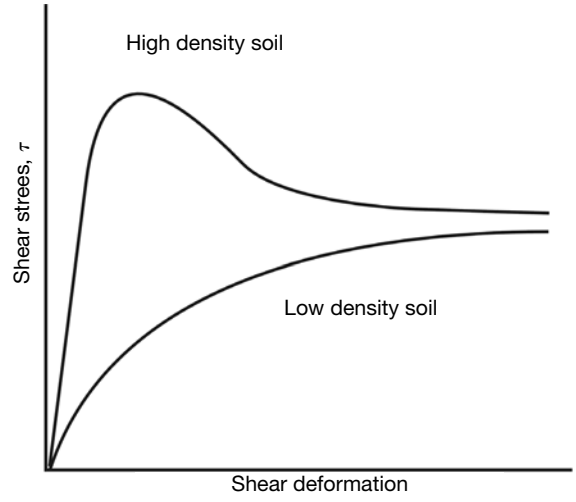

FIGURE 2A.31 Stress deformation for a soil.

2A.8.2.2 Triaxial Testing of Soil

With clays, the time to achieve drainage is important. In the direct shear test, the soil is initially loaded with a total vertical stress. The pore pressure generated by this load may be allowed to dissipate, permitting consolidation to occur. With time, substantially all of the pore pressure is dissipated; the soil reaches an equilibrium volume under the total stress, which is now an effective stress since no pore pressures exist.

The triaxial shear apparatus has proven to be superior to the direct shear box for the study of the

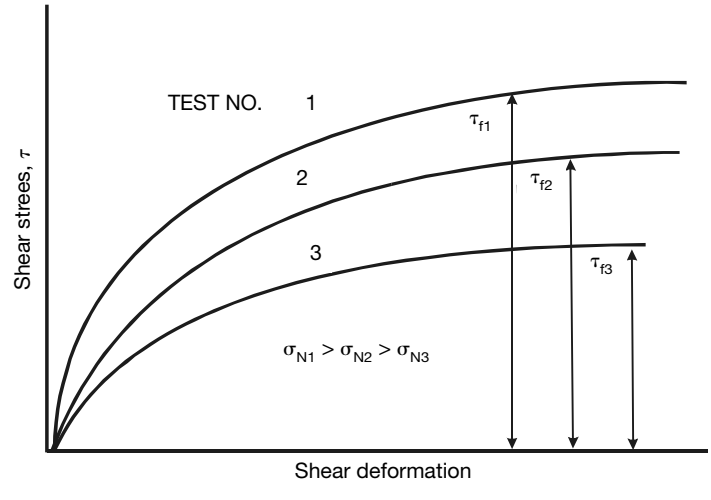

FIGURE 2A.32 Stress-deformation curves for direct shear test at differing vertical stresses.

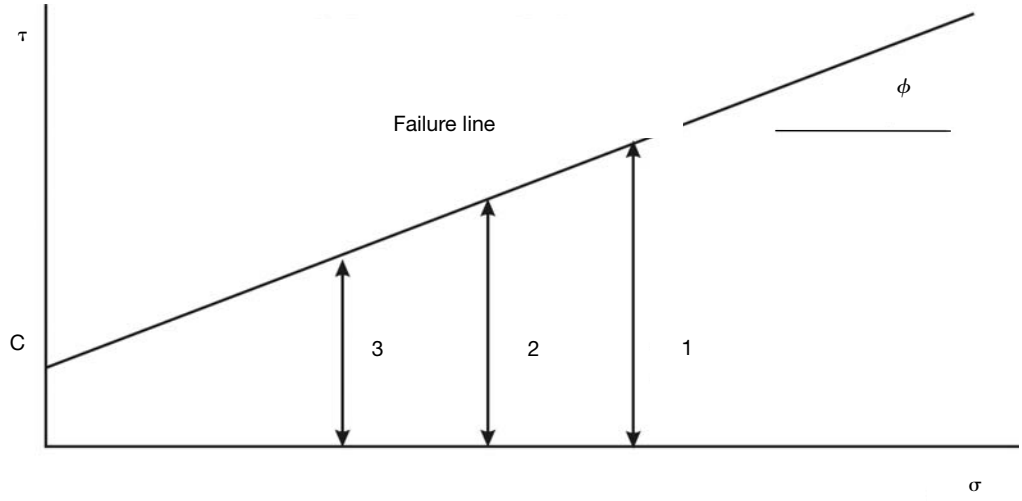

FIGURE 2A.33 Failure diagram for a soil test in direct shear.

consolidated undrained shear strength of a clay primarily because of its ability to control and monitor internal pore water pressures. Preceding the discussion of consolidated undrained shear strength, Mohr's stress theory and the mechanics of the triaxial test must be discussed.

2A.8.2.2.1 Stresses at a Point. Mohr's theory of stresses is fully explained in texts on mechanics of materials. However, that part of the theory pertinent to soil mechanics will be reviewed. Compressive stress will be considered positive, since stresses in soils generally are compressive and not tensile. Shear stresses tending to cause counterclockwise rotation will be defined as positive as well. Consider the stresses on a small two-dimensional element shown as Fig. 2A.34(A). If a plane at an angle (is passed through the element, there exist two resulting stresses on

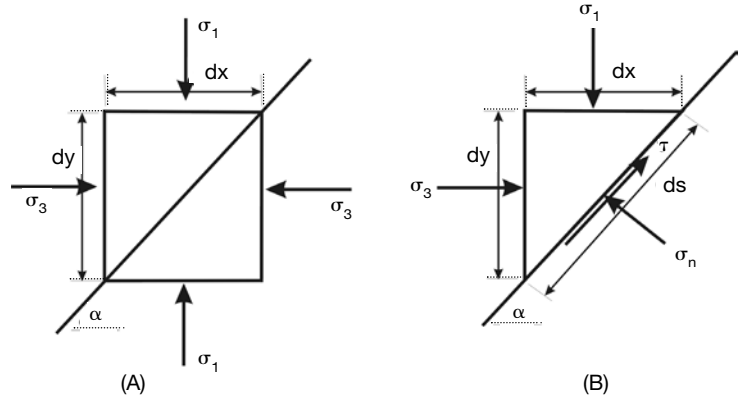

FIGURE 2A.34 Stress on a differential element.

that plane required for stability of the element (Fig 2A.34(A)). σ is the component of the resultant stress on a plane that acts at right angles to the plane, i.e., a normal stress. τ is the component of the resultant stress that is parallel to the plane, i.e., the shearing stress. σ_1 is the maximum normal stress on any plane through the point under consideration. There is no shearing stress on this plane. σ_3 is the minimum normal stress on any plane through the point under consideration. There is no shear stress on this plane. σ_3 acts at right angles to σ_1. σ_2 is the normal stress acting on a plane at right angles to the planes on which σ_1 and σ_3 act. There is no shear stress in this plane. By definition σ_2 may not exceed the magnitude of σ_1 nor may it be less than σ_3. σ_1, σ_2, and σ_3 are called principal stresses. They are orthogonal; that is, they act at right angles to one another.

If we consider Fig. 2A.34, we can determine the relationship between the normal and shear stresses, σ_n and τ, on a plane inclined at an angle α to the major principal plane, and the major and minor normal stresses, σ_1 and σ_3:

$$\tau = \frac{\sigma_1 - \sigma_3}{2} \sin 2\alpha$$
$$\sigma = \frac{\sigma_1 + \sigma_3}{2} + \frac{\sigma_1 - \sigma_3}{2} \cos 2\alpha \tag{2A.64}$$

These two equations allow the calculation of the stresses σ and τ on any plane inclined at an angle α to the plane of the major principal plane when σ_1 and σ_3 are known.

This can also be accomplished graphically using Mohr's circle. The ordinates represent shear stress and the abscissa, normal stresses (see Fig. 2A.35).

2A.8.3.2 Triaxial Tests

The direct shear test does not lend itself to the measurement of soil pore pressures, and the test has several other disadvantages. The triaxial test has become a popular method to determine the shear properties of a soil. The triaxial apparatus is shown in Fig. 2A.36.

Triaxial tests are performed in two stages. The first stage subjects the sample to a system of normal stresses (Fig. 2A.37). Usually, this is done by application of an all-around cell pressure

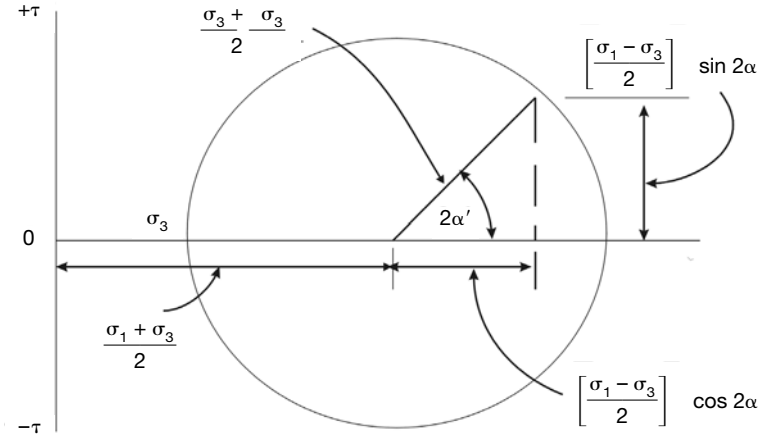

FIGURE 2A.35 Mohr's circle representation of stress on a differential element.

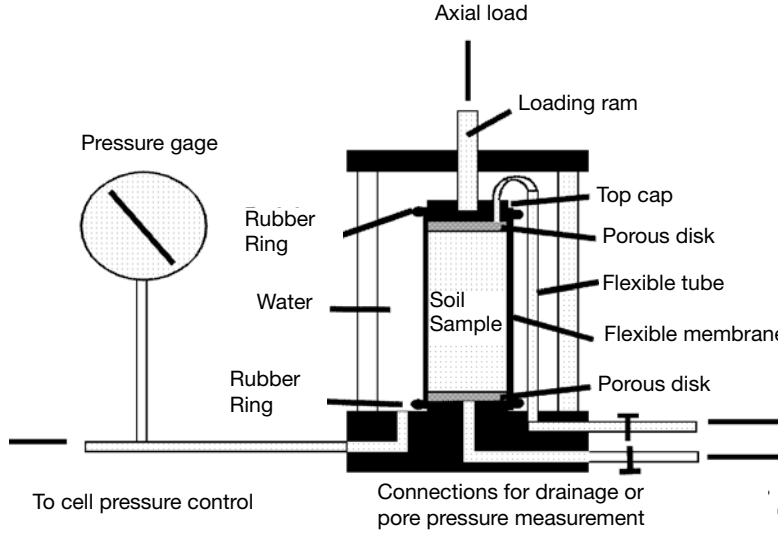

FIGURE 2A.36 Schematic of triaxial test equipment.

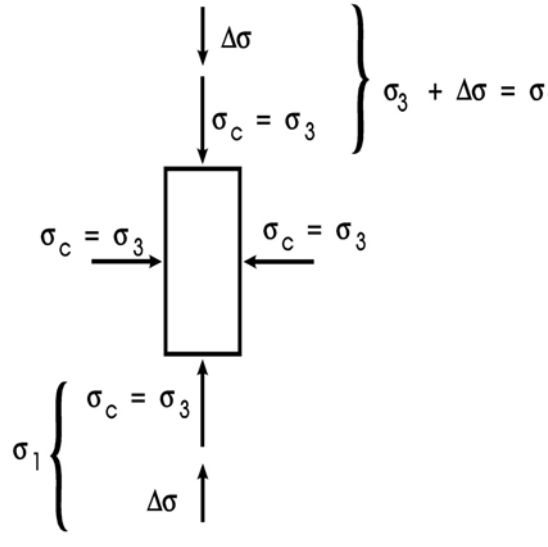

FIGURE 2A.37 Triaxial stresses on specimen.

($\sigma_c = \sigma_3$), in which case the stress acts in all directions. If the drainage passage from the porous stone is opened, the sample may be allowed to consolidate under the stresses applied during the first stage. Alternatively, it may be desired to prevent drainage during the first stage. Stage one can then be either *consolidated* or *unconsolidated*.

In the second stage, an axial stress ($\Delta\sigma$) may be applied to the sample through the loading piston. Again, drainage may or may not be permitted. Stage two may then be either *drained* or *undrained*.

Assuming isotropic stresses are applied in stage one, three types of tests are commonly performed on a soil sample.

2A.8.3.2.1 Consolidated Drained Test. In the first stage of this test, the soil is permitted to consolidate completely under the influence of the cell pressure. If the sample is saturated, the drainage connection from the porous stone may be connected directly to a burette. The progress of consolidation may be followed by measurement of the water outflow from (or inflow to) the sample. When consolidation is complete, with no further drainage from or into the sample, the second stage may proceed. An axial strain that causes a stress is applied so slowly that the pore pressures generated by the shear are permitted to dissipate. In the literature this test is commonly called a consolidated drained test (CD Test), a drained test, a slow test, or a S test.

2A.8.3.2.2 Consolidated Undrained Test. In this test, stage one is performed identically to stage one of the preceding test. In the second stage, drainage connections are closed as the sample is sheared to failure under undrained conditions. This test is called a consolidated undrained test (CU Test), a consolidated quick test (CQ or QC Test), or a R test.

2A.8.3.2.3 Unconsolidated-Undrained Test. In this test, the soil is not permitted to consolidate under the cell pressure, nor is drainage permitted during the shearing stage. This test is known as an unconsolidated undrained test (UU Test), a quick test, or a Q-Test.

2A.8.3.3 The Consolidated Drained Strength of Saturated Normally Consolidated Clay

Since, in this test, no pore pressures are allowed to build up, the stresses in the soil specimen are effective stresses. These stresses can easily be measured or calculated from the measured forces.

In the first stage, the soil is permitted to consolidate completely under the influence of the cell pressure. Mohr's circle for both total and effective stress is a single point along the σ axis with a value equal to the cell pressure, or σ_3.

During the second stage, shear stress is slowly applied by the piston. The applied stress ($\Delta\sigma$) is equal to the diameter of Mohr's circle. The cell pressure, equal to the minor principal stress (σ_3), is not varied during the course of the shear test. The progress of shear can be shown as a series of Mohr's circles increasing in diameter, anchored at their left side on the value of the cell pressure (Figure 2A.38).

For a single test, a plot of stress difference versus axial strain is shown in Fig. 2A.39. Points 1 through 5 in Fig. 2A.39 show values of the stress difference used to obtain the five Mohr's circles shown in Fig. 2A.38. It is obvious that the stress difference causes a shear stress so that the similarity of results to those obtained by direct shear is not surprising.

If a series of drained triaxial shear tests are performed on a normally consolidated soil with the consolidation (cell) pressure varied from test to test, a plot of the Mohr's circles for the maximum stress differences might appear as in Fig. 2A.40.

An envelope line, enclosing all possible Mohr's circles for this normally consolidated, saturated clay soil, will be a straight line and will pass through the origin when extended backward. The angle of inclination of this line is $\bar{\phi}$, approximately equal to the friction angle as measured in the drained direct shear test. The physical interpretation of this is that the shear strength is directly proportional to the consolidation pressure, i.e.,

$$s = t_f = \bar{\sigma} \tan\bar{\phi} \tag{2A.65}$$

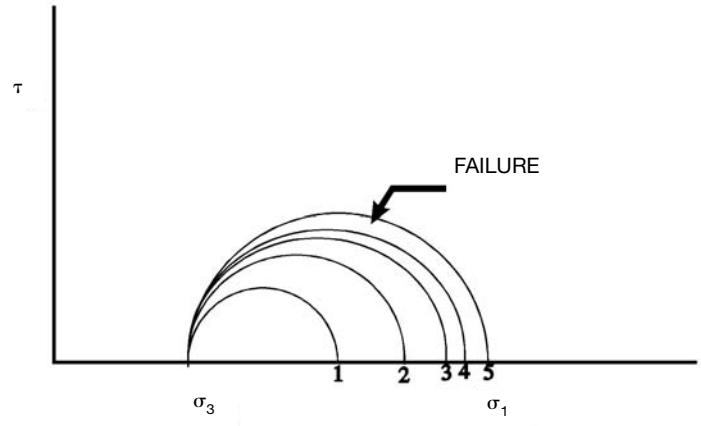

FIGURE 2A.38 Mohr's circles for increasing axial stress.

There is a failure on one plane in the triaxial sample, and this failure is on a plane theoretically represented by the point of tangency of Mohr's circle and the envelope.

2A.8.3.4 Consolidated Undrained Strength of Saturated Normally Consolidated Clay

In the consolidated undrained test, the first stage proceeds in the same manner as the consolidation phase of the consolidated drained triaxial test. The soil is consolidated to an isotropic (all-around) stress equal to the cell pressure. For the sample to remain normally consolidated, the cell pressure

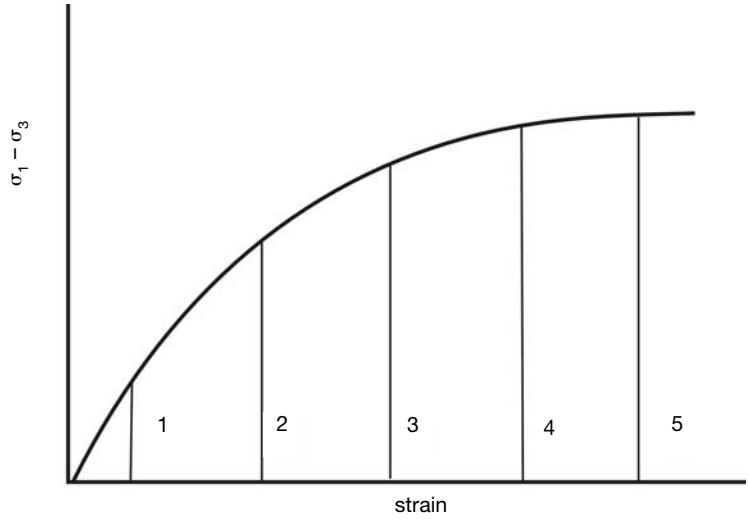

FIGURE 2A.39 Stress difference versus strain for triaxial S test on normally consolidated clay.

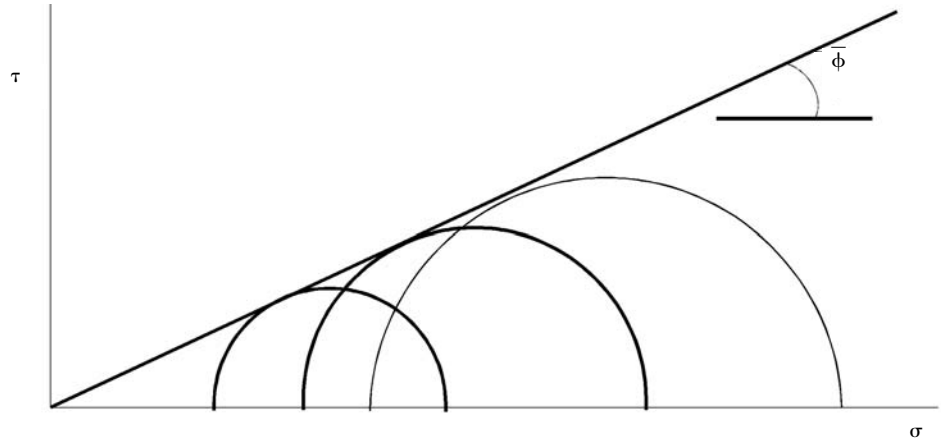

FIGURE 2A.40 S-test envelope for normally consolidated clay.

must exceed the consolidation pressure of the soil in the ground. If plotted on a Mohr's diagram, at the end of the consolidation phase, the stresses would plot as a point circle along with the σ axis, since, as with the drained test, the progress of consolidation may be monitored. Upon completion of consolidation, the shear phase begins. To maintain an undrained condition, drainage from this sample is prevented. Since no water leaves the system, the shearing occurs at constant volume.

A volume change versus strain curve is not appropriate because there is zero volume change at all strains. On the Mohr's diagram, Fig. 2A.41, one may see that the diameter of the failure circle for the undrained test is about half the diameter of the failure circle for the drained case at the same consolidation stress.

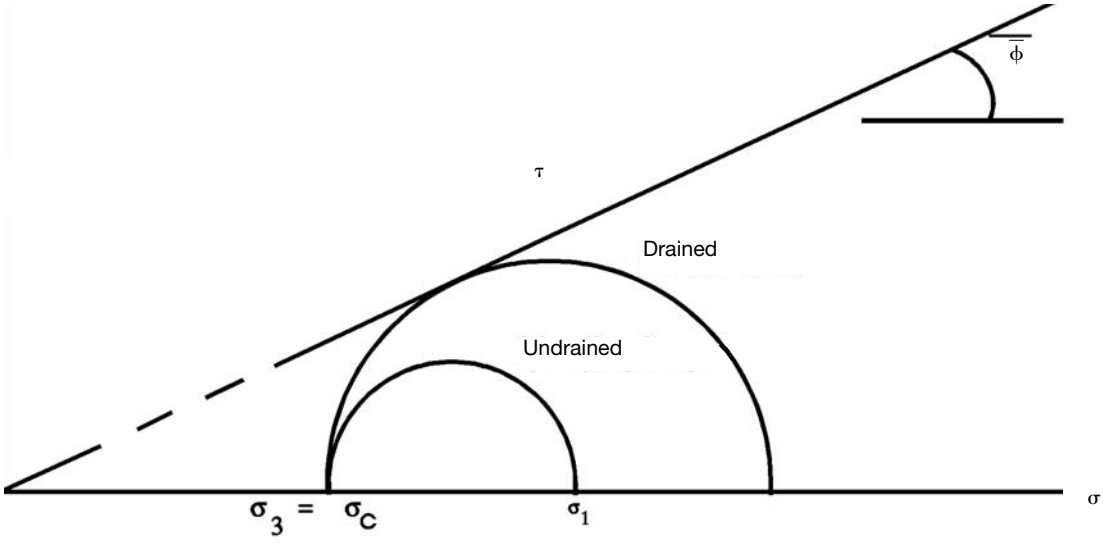

FIGURE 2A.41 Mohr's circle for undrained test compared to drained test.

A second sample is consolidated to a higher stress and sheared under constant volume. The corresponding Mohr's circle (Fig. 2A.42) shows a proportionately larger failure circle, but again, only about one half the diameter of the drained failure circle at the higher consolidation stress. Since this proportionality exists, one may draw a failure envelope.

This envelope is also a straight line, which can be traced backward through the origin. It is known as the R or CU envelope. The dotted line portion shows extrapolation back to the origin, at stresses below the field consolidation pressure of the soil. If, in the laboratory, a sample had been consolidated to a stress less than the field consolidation stress, it would no longer be normally consolidated since stresses were at one time greater than now. Its strength would also be slightly greater than shown by the dotted line, as will be explained in the section on overconsolidated soils.

With only a simple adjustment to the R test, one can obtain a great deal more data. Instead of closing the drainage connection to the base of the sample, if, at the end of consolidation, a pore pressure transducer is placed in the line, one can still run a test essentially undrained during the shearing phase. But the pore pressures caused by the shearing can be constantly monitored. This test is known as the R (R-bar) test.

After consolidation, as the soil is sheared under the stress difference, there is a tendency for the soil to decrease in volume as with the drained test. But drainage is prevented; water cannot leave the soil. The pore water pressure gradient that existed to move the water out of the soil is now permitted to build up. A positive pore water pressure is generated and is measured by the transducer. Typical stress and porewater pressure versus strain curves are shown in Fig. 2A.43.

During drained shear it was not necessary to differentiate between total stresses and effective stresses. The pore pressures were zero; total stresses were equal to the effective stresses and a single Mohr's circle results.

For the R test, the consolidation phase (which implies full drainage) yields a single point Mohr's circle equal to the cell pressure. However, the moment the undrained shear begins, pore pressures are generated and

$$\begin{aligned} \bar{\sigma}_1 &= \sigma_1 - u \\ \bar{\sigma}_3 &= \sigma_3 - u \end{aligned} \tag{2A.66}$$

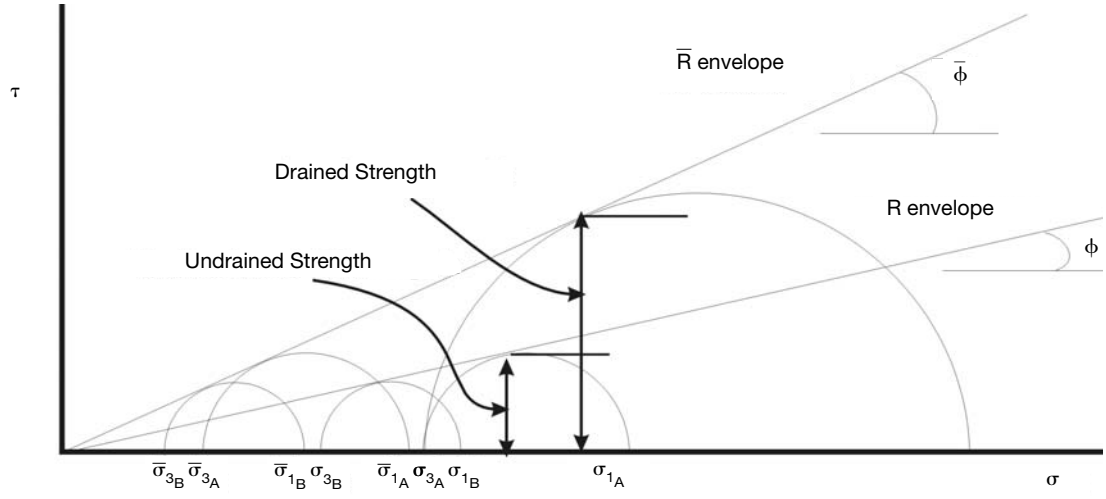

FIGURE 2A.42 Mohr's circles for increasing consolidation pressures in the undrained test.

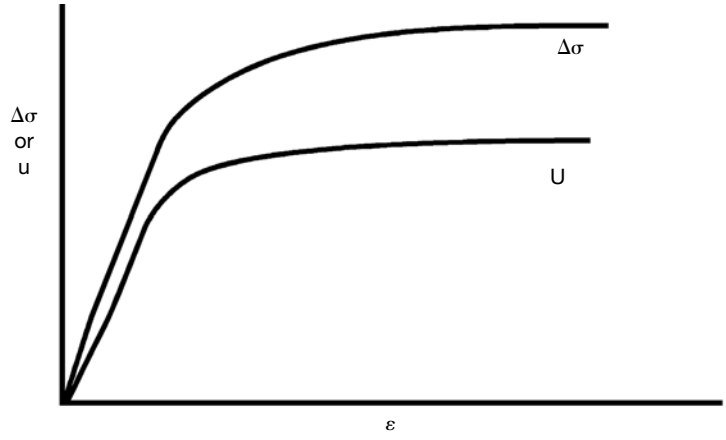

FIGURE 2A.43 Typical stress and pore pressure versus strain in undrained shear.

Since the cell pressure is constant and equal to σ_3 in the triaxial compression test, the total stress Mohr's circles are anchored on the left at $\sigma_3 = \sigma_c$, just as in the drained test. However, the effective stress σ_3 becomes less than the cell pressure by the magnitude of pore pressure generated. Since pore pressure constantly increases with shear, the effective stress Mohr's circles are constantly shifting to the left, i.e., σ_3 is constantly decreasing. For any given time or strain, there are two Mohr's circles, a total stress circle with $\sigma_3 = \sigma_{cell}$ and an effective stress circle with σ_3 and σ_1, displaced leftward (reduced) by the amount of the generated pore pressure at that time or at that given strain. Fig. 2A.44 illustrates this.

The total stress Mohr's circle will have the same diameter as the effective stress circle:

$$\begin{aligned} \Delta\sigma = \overline{\sigma}_1 - \overline{\sigma}_3 &= \text{diameter of Mohrs circle} \\ &= (\sigma_1 - u) - (\sigma_3 - u) \\ &= \sigma_1 - u - \sigma_3 + u \\ &= \sigma_1 - \sigma_3 \end{aligned} \tag{2A.67}$$

The effective stress and total stress Mohr's circles will be identical in size and all points on the effective stress circle are simply displaced by the magnitude of the pore pressure.

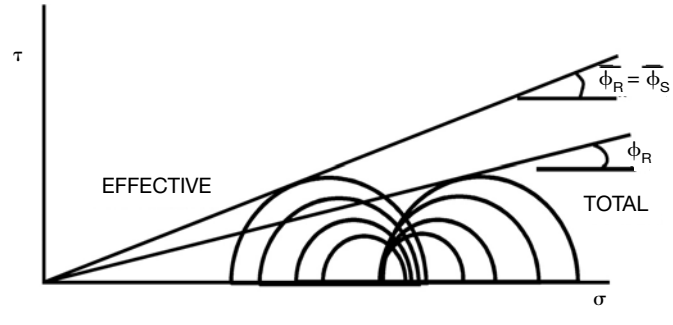

FIGURE 2A.44 Total and effective stress circles for undrained test.

In Fig. 2A.44 note that shear continues until the effective stress Mohr's circle touches the effective stress envelope. This envelope is essentially the same as the drained envelope.

In the drained direct shear test, the normal effective stress remains constant as shear stress is increased to failure. In the drained triaxial test, normal effective stress on the potential plane of failure increases slightly as shear stresses increase rapidly. In the consolidated undrained triaxial test, normal effective stresses generally decrease somewhat due to generation of pore pressures while shear stresses increase to failure.

It should be quite clear now that effective stresses at failure govern the strength of a soil. For a given normally consolidated clay, the effective normal stress on a potential failure plane governs the shear strength of the soil, both drained and undrained. Even though this effective stress concept is relatively simple to explain, in practice we more often wish to relate the strength to stresses *before* shearing. Relating undrained strength to consolidation pressure before shearing is more useful for engineering predictions.

Previously, the results of performing R tests (without pore pressure measurement) on two samples consolidated to different pressures were explained. We now perform two R tests (with pore pressure measurement) on samples consolidated to different pressures. Results are shown in Fig. 2A.45 and Fig. 2A.46. Note that the total stress circles, with σ_3 equal to the cell pressures, form the R envelope. The effective stress circles each touch the R or effective stress envelope which is essentially the same envelope as would be obtained from drained tests. Note also that for the larger consolidation pressure, larger pore pressures are generated. With increasing consolidation pressure, Mohr's circle at failure (the shear strength) increases proportionately, as does the failure pore pressure, which is shown by the offset of the effective stress circle from its total stress circle. In each case, the offset is approximately equal to the diameter of Mohr's circle. Only the R envelope represents a failure line, where stresses become critical on a plane on which a given effective stress acts. The R envelope is simply an envelope enclosing the maximum size Mohr's circle.

Sometimes the R envelope is called a total stress envelope. This leads to confusion. Total stress conditions are meaningless unless they are related to effective stresses. In the case of the R envelope, it is an envelope of total stresses at undrained failure only if and when the σ_3 of the failure cir-

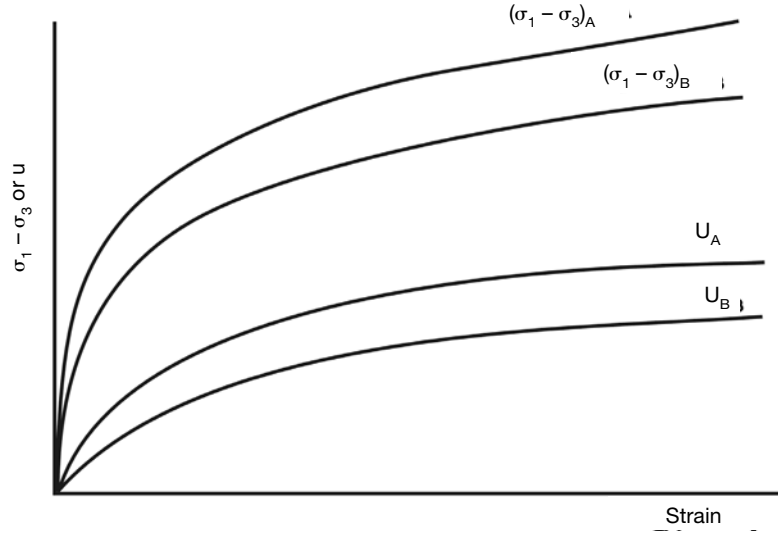

FIGURE 2A.45 Stress and pore pressure versus strain for two tests at two consolidation pressures.

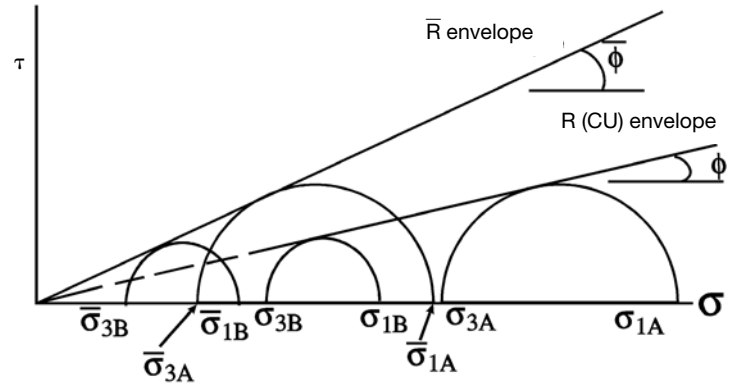

FIGURE 2A.46 Mohr's circles for two tests.

cle is the consolidation pressure of the sample. In this way it bears a fixed relationship to effective stresses.

Figure 2A.46 also shows, for a given consolidation pressure, the drained strength and failure circle, and both the undrained failure circles and the undrained strength. Now a main advantage of the R̄ test becomes evident. From the R̄ envelope, we can predict the drained strength of a soil at any given consolidation pressure. The R̄ test gives predictions of both the drained and undrained strengths. Moreover, the drained test requires a very slow shear rate so that pore water pressures generated in the failure zone can migrate from the sample. The R test still requires time for pore pressures in the failure zone to equilibrate throughout the sample, but the time involved is substantially less than the time for full drainage.

From the foregoing we can conclude that for a normally consolidated saturated clay (constant stress history) for the drained condition, shear strength is directly proportional to the consolidation pressure. For the undrained case, the same is true, but the constant of proportionality is reduced to tan ϕ.

2A.8.3.5 Unconsolidated Undrained Test and Unconfined Compression Test of Normally Consolidated Clay

The undrained strength of the soil in this test is also directly proportional to the consolidation pressure, which is the consolidation pressure of the soil in the ground.

In this test there is no drainage allowed and hence no volume change in the specimen can occur. Consequently, when the sample is sheared, identical effective stress circles will develop no matter what the value of the cell pressure. At failure, the strength will also be the same for all tests. The failure total stress circle will be the same size as the effective stress circle, but displaced by the greater pore pressure (Fig. 2A.47). A Mohr's plot for total stresses for the UU tests have resulted in a series of circles of the same diameter. The UU envelope, with respect to total stresses, has a ϕ of zero and cohesion intercept, c. There may be a number of total stress circles, but only one effective stress circle and this one is governed by the common consolidation pressure.

Both the cost of triaxial apparatus and the requirement for highly skilled labor used in triaxial testing are large. Since the strength of the UU sample was dependent only on the consolidation stress in the ground and independent of the cell pressure, the use of a zero confining stress would be obvious. It dispenses with the need for much of the triaxial apparatus and should result in a Mohr's circle of equal size by the $\phi = 0$ principle. If we perform such a test, called the unconfined compression test, ideally the resulting Mohr's circle is of size equal to those failure circles produced by the unconsolidated undrained test (Fig. 2A.48). In such a test, we cannot measure pore pressures, so the

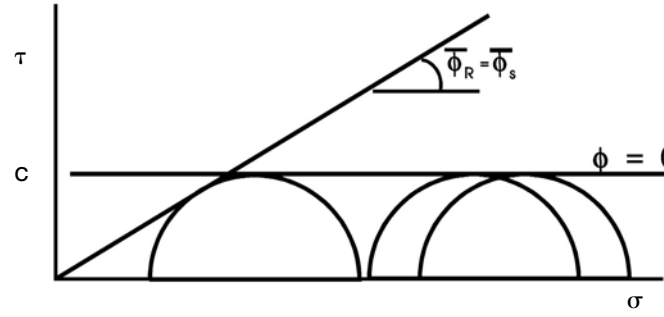

FIGURE 2A.47 Total and effective stress circles for the UU test.

position of the failure effective stress circle cannot be established. Although we have deduced the radius of the effective stress Mohr's circle (it is the same as the total stress circle radius), we cannot know what is the effective stress friction angle of the soil. The radius is also half the diameter of the circle, which is the unconfined compressive strength, q_u, which in turn is σ_1 at failure when σ_3 is zero. In general then, for undrained shear strength of cohesive soils:

$$s = \tau_f = c = \frac{q_u}{2} = \frac{\Delta\sigma}{2} \tag{2A.68}$$

2A.8.3.6 Shear Strength of Saturated Overconsolidated Soil

A reconsolidated or overconsolidated soil is one which, at some time in its geologic history, has had acting on it a consolidation pressure greater than that presently acting on it. Consolidation, of course, implies complete drainage and transfer of total stresses to the effective stresses of the soil skeleton. The causes of the preconsolidation and subsequent removal of effective stress might have been by deposition and subsequent erosion, a glacial load and melting, desiccation with subsequent more humid conditions, or any of the other causes discussed when the subject of consolidation was treated.

Fig. 2A.49 shows, on a natural scale of void ratio versus effective stress, a soil normally consolidated to point C and unloaded to point E. This plot is similar to the usual consolidation curve except that is shown as the effective stress on a natural scale and not log p, effective stress plotted on a log-

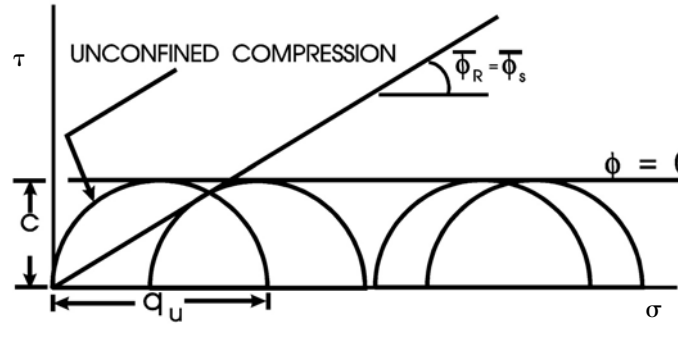

FIGURE 2A.48 UU envelope and unconfined compression, Mohr's circle.

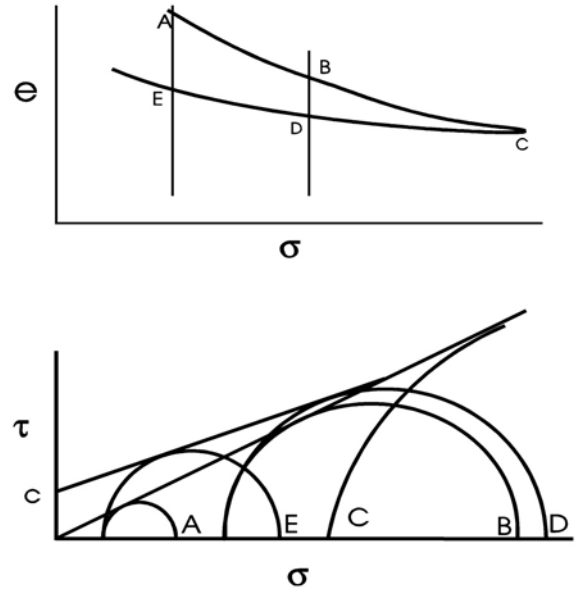

FIGURE 2A.49 Volume change and Mohr's circle plots for overconsolidated soils.

arithmic scale. What would be a relatively straight line on a logarithmic plot will be shown concave upwards on an arithmetic plot. This curve is a consolidation curve, even though the data were obtained from triaxial consolidation tests where $\sigma_1 = \sigma_2 = \sigma_3$.

In Fig. 2A.49, circles A, B, and C are for soils that are normally consolidated. Points D and E correspond to the consolidation pressures of B and A, respectively, but each of these soils has been reconsolidated to the stress level of C. Fig. 2A.49 shows Mohr's failure circles for soils A–E for the consolidated drained condition. The diameter of the failure circles and the shear strength of the soil are directly proportional to the consolidation pressure, which is the σ_3 of the drained failure circles.

It should be expected that density expressed as void ratio and effective consolidation stress will control the strength of these soils. Soil D has been consolidated to the same effective stress as soil B. Soil D, however, is shown in Fig. 2A.49 to be denser, to have a lower void ratio than B. It would therefore be expected that D will be stronger than B. Fig. 2A.49 shows that this is so.

Soil E is denser than A, and both have been consolidated to the same effective stress level. Soil E was at one time reconsolidated (with drainage, of course) to the stress level of C. In rebound, it had only a slightly greater void ratio than C. The ratio of the σ_3 of E and the σ_3 of C is the overconsolidation ratio, which is shown to be on the order of eight or so. Again, soil E is stronger than A, as denoted by the larger Mohr's failure circle.

In comparing the failure circles, consolidation stresses, and void ratios it is apparent that the strength of these soils is controlled more by effective consolidation stresses than by void ratios.

The failure envelope through the origin and tangent to Mohr's circles A, B, and C was previously introduced as the drained strength envelope for a normally consolidated clay, or the S envelope. It indicates that the shear strength is directly proportional to the effective consolidation pressure and in particular to the consolidation pressure on the plane of failure, i.e., where the Mohr's circle touches the envelope.

The failure envelope for soils C–E, the soils that have been reconsolidated to the stress level of C, is not strictly a straight line; it is curved downward slightly and does not pass through the origin.

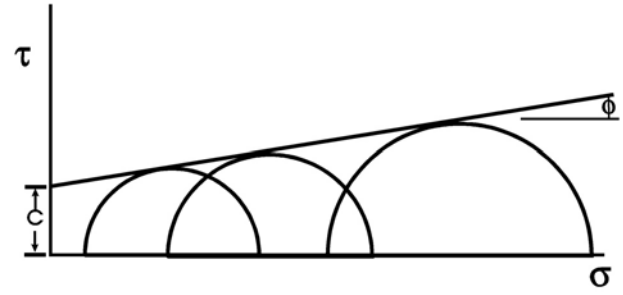

FIGURE 2A.50 Overconsolidated soil Mohr's envelope.

It joins the ϕ_ss envelope for normally consolidated soil at the point where the failure circle for C is tangent to the normally consolidated failure circle. When tests are performed on a reconsolidated soil, the final consolidation pressures generally are in a relatively narrow range and are generally substantially less than the preconsolidation pressure. In this range, it is customary to fit a straight line to the circles obtained from the tests. Such a line will have a slope expressed as a ϕ angle and will have a cohesion intercept c. Fig. 2A.50 shows such an effective stress envelope.

It can be concluded that the greater the preconsolidation pressure, the higher is the envelope, and therefore the greater is c in the expression $\tau = c + \sigma \tan\phi$. It can be seen also that c and ϕ are not material properties of a soil.

Typical stress–strain and volume change–strain properties of heavily reconsolidated soils are shown in Fig. 2A.51 and Fig. 2A.52, respectively. The soil behaves very much the same as does a dense sand, having a peak shearing resistance at low strain, and dilating or expanding in volume at strains greater than those mobilized at the peak strength.

2A.9 CORRELATIONS BETWEEN SOIL INDEX PROPERTIES AND FOUNDATION DESIGN PARAMETERS

Often, high-quality laboratory shear strength data is unavailable, at least for preliminary studies. Consequently, it is necessary to estimate shear strength parameters from other, less rigorous evalua-

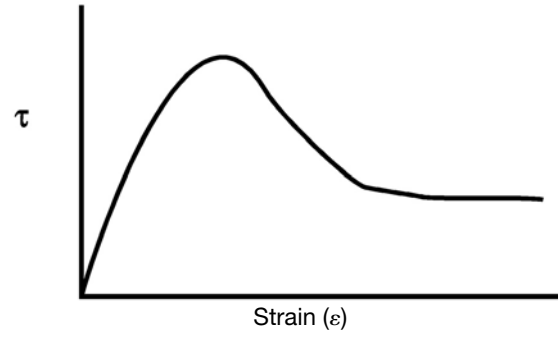

FIGURE 2A.51 Stress–strain for overconsolidated clay.

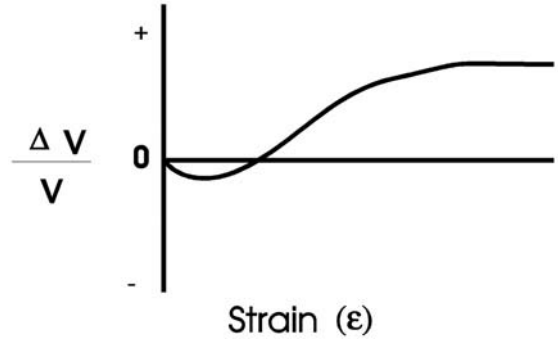

FIGURE 2A.52 Strain–volume change for overconsolidated clay.

tion. Methods for evaluating effective stress friction angles from soil index properties are presented below.

2A.9.1 Effective Stress Friction Angle of Cohesionless Soils

Many researchers have presented correlations for estimating the effective stress friction angles for cohesionless soils. These correlations are usually with soil type, relative density, and unit weight or void ratio. Fig. 2A.53 shows a general relationship between effective stress friction angle and dry density.

2A.9.2 Effective Stress Friction Angle of Cohesive Soils

Correlations for effective stress friction angles for cohesive soils are generally limited to normally consolidated soils and remolded clays and residual (large strain) friction angles. Mitchell[14] published the following correlation for normally consolidated soils:

$$\sin \varphi \approx 0.8 - 0.094 \ln(PI) \tag{2A.69}$$

where φ = effective stress friction angle for normally consolidated soil
PI = Plasticity Index

Fig. 2A.54 illustrates the typical changes in the residual friction angle for soils at the Amuay landslide site with changes in effective stress and plasticity. P_a is the atmospheric stress in appropriate units.

2A.9.3 Undrained Shear Strength of Cohesive Soils

The undrained shear strength, s_u, is probably the most widely used parameter for describing cohesive soils. It is affected by the type of test used, boundary conditions, rate of loading, and confining stress level. Skempton suggested the following correlation for normally consolidated soil, s_u, from the field vane shear test:

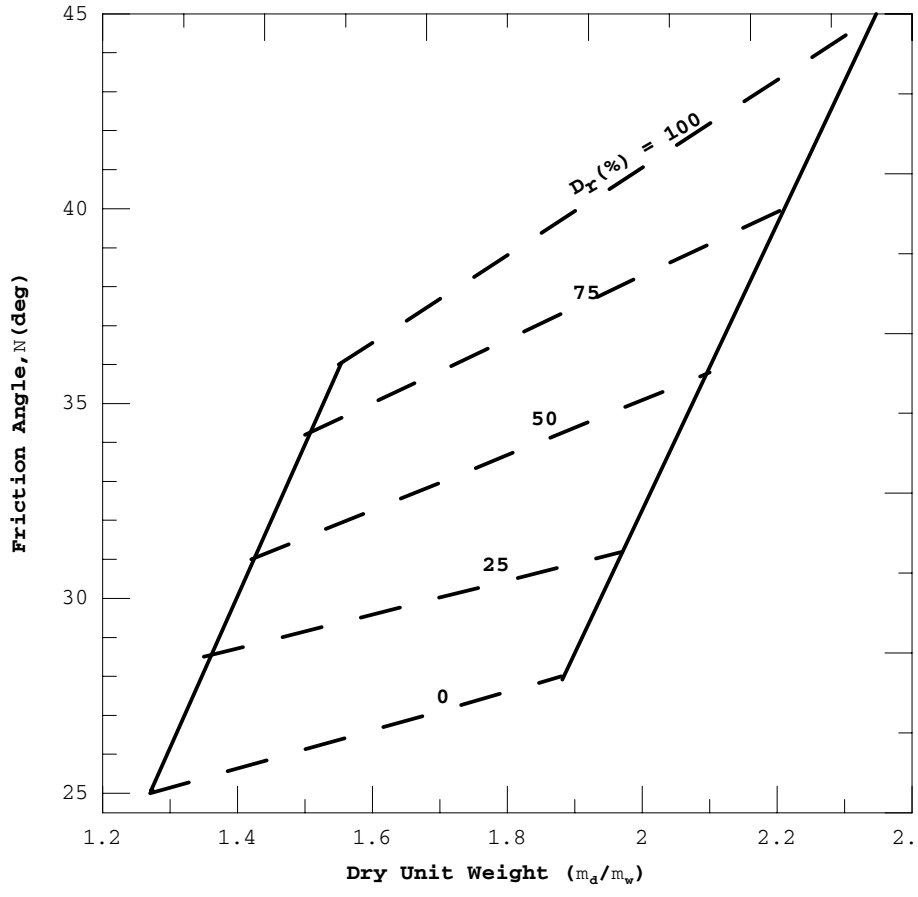

FIGURE 2A.53 Friction andgle versus relative density and unit weight.

$$\sigma_u/\overline{\sigma}_{vo} = 0.11 + 0.037PI \tag{2A.70}$$

Chandler[15] modified this equation to take into account the preconsolidation stress (σ_p):

$$\frac{s_u}{\overline{\sigma}_p} = 0.11 + 0.0037PI \tag{2A.71}$$

The accuracy is said to be ±25%.

Similarly, Jamiolkowski et al.[16] Provided the following equation for low to moderate PI soils:

$$\frac{s_u}{\overline{\sigma}_{vo}} \approx (0.23 \pm 0.04)OCR^{0.8} \tag{2A.72}$$

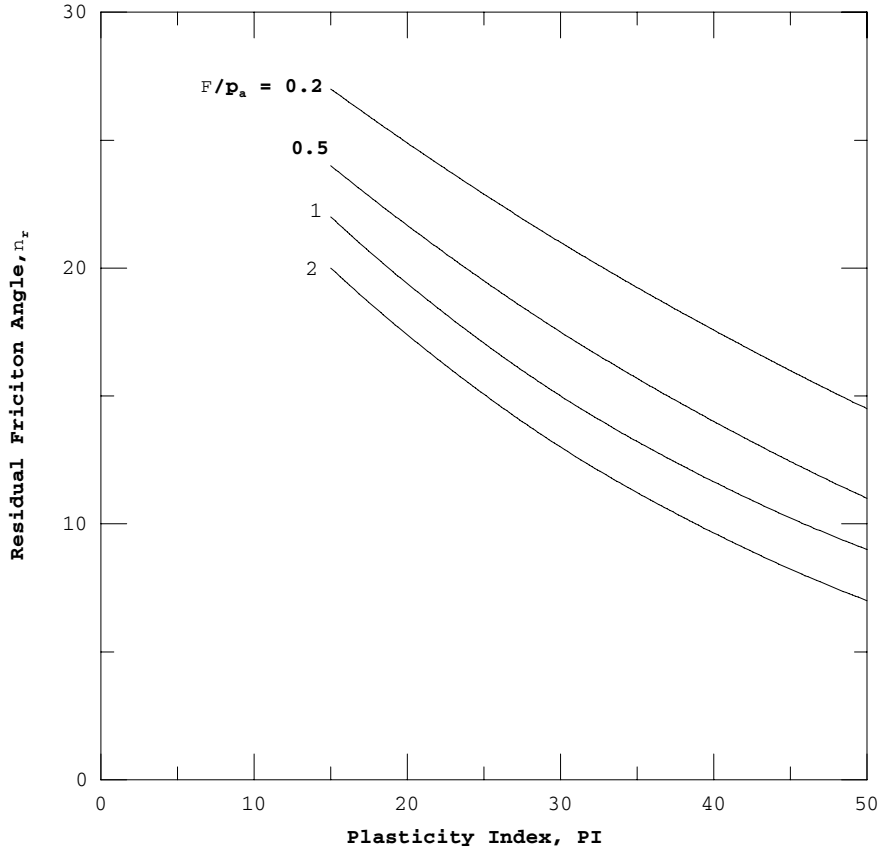

FIGURE 2A.54 Residual friction angles for Amuay landslide soils versus PI and effective normal stress.

2A.10 REFERENCES AND FURTHER READING

1. Atterberg, A., "Lerornas Forhallande till Vatten, deras Plasticitetsgranser och Plasticitetsgrader," *Kangliga Lantbruksakademiens Handlinigar och Tidskrivt,* Vol. 50, No. 2, pp. 132–158 (1911).
2. Casagrande, A. "Research on the Atterberg Limits of Soils," *Public Roads,* Vol. 13, No. 8, pp. 121–136 (1932).
3. Skempton, A. W., "Notes on the Compressibility of Clays," *Quarterly Journal of the Geological Society of London*, pp. 119–135 (1944).
4. Esrig, M. I., unpublished notes (1968).
5. Terzaghi, K., "Influence of Geological Factors on the Engineering Properties of Sediments," *Harvard Soil Mechanics Series No. 50*, Cambridge, Massachusetts (1955).
6. Casagrande, A., "Classification and Identification of Soils," *Transactions,* ASCE, Vol. 113, pp. 901–930 (1938).
7. Carpenter, G. W., and R. W. Stephenson, "Permeability Testing in the Triaxial Cell," *ASTM Geotechnical Testing Journal*, Vol. 9, No. 1, March (1986).
8. Boussinesq, J., *Application des Potentiels a L'Etude de L'Equilibre et du Mouvement des Solides Elastiques,* Gauthier-Villars, Paris (1885).

9. Casagrande, A., "The Determination of the Pre-Consolidation Load and Its Practical Significance," discussion D-334, *Proceedings of the First International Conference on Soil Mechanics and Foundation Engineering,* Cambridge, Vol. III, pp. 60–64 (1936).
10. Rutledge, P. C., "Relation of Undisturbed Sampling to Laboratory Testing," *Transactions,* ASCE, Vol. 109, pp. 1162–1163 (1944).
11. Schmertmann, J. H., "The Undisturbed Consolidation Behavior of Clay," *Transactions,* ASCE, Vol. 120, pp. 1201–1233 (1955).
12. Taylor, D. W., *Fundamentals of Soil Mechanics,* Wiley, New York (1948).
13. Casagrande, A., and Fadum, R. E., Closure to "Applications of Soil Mechanics in Designing Building Foundations," *Transactions,* ASCE, Vol. 109, p. 467 (1944).
14. Mitchell, J. K., *Fundamentals of Soil Behavior*, Wiley, New York (1976).
15. Chandler, R. J., "The In-Situ Measurement of the Undrained Shear Strength of Clays Using the Field Vane," *Vane Shear Strength Testing in Soils: Field and Laboratory Studies* (STP 1014), ASTM, Philadelphia (1988).
16. Jamiolkowski, M., Ladd, C. C., Germaine, J. T., and Lancellotta, R., "New Developments in Field and Laboratory Testing of Soils," *Proceedings, 11th International Conference on Soil Mechanics and Foundation Engineering*, Vol. 1, San Francisco (1985).